ACS Catalysis

pubs.acs.org/acscatalysis

Research Article

Chimeric Cellobiose Dehydrogenases Reveal the Function of Cytochrome Domain Mobility for the Electron Transfer to Lytic Polysaccharide Monooxygenase

Alfons K. G. Felice, Christian Schuster, Alan Kadek, Frantisek Filandr, Christophe V. F. P. Laurent, Stefan Scheiblbrandner, Lorenz Schwaiger, Franziska Schachinger, Daniel Kracher, Christoph Sygmund, Petr Man, Petr Halada, Chris Oostenbrink, and Roland Ludwig*

Cite This: *ACS Catal.* 2021, 11, 517−532

Read Online

ACCESS | Metrics & More | Article Recommendations | Supporting Information

ABSTRACT: The natural function of cellobiose dehydrogenase (CDH) to donate electrons from its catalytic flavodehydrogenase (DH) domain via its cytochrome (CYT) domain to lytic polysaccharide monooxygenase (LPMO) is an example of a highly efficient extracellular electron transfer chain. To investigate the function of the CYT domain movement in the two occurring electron transfer steps, two CDHs from the ascomycete *Neurospora crassa* (*Nc*CDHIIA and *Nc*CDHIIB) and five chimeric CDH enzymes created by domain swapping were studied in combination with the fungus' own LPMOs (*Nc*LPMO9C and *Nc*LPMO9F). Kinetic and electrochemical methods and hydrogen/deuterium exchange mass spectrometry were used to study the domain movement, interaction, and electron transfer kinetics. Molecular docking provided insights into the protein−protein interface, the orientation of domains, and binding energies. We find that the first, interdomain electron transfer step from the catalytic site in the DH domain to the CYT domain depends on steric and electrostatic interface complementarity and the length of the protein linker between both domains but not on the redox potential difference between the FAD and heme *b* cofactors. After CYT reduction, a conformational change of CDH from its closed state to an open state allows the second, interprotein electron transfer (IPET) step from CYT to LPMO to occur by direct interaction of the *b*-type heme and the type-2 copper center. Chimeric CDH enzymes favor the open state and achieve higher IPET rates by exposing the heme *b* cofactor to LPMO. The IPET, which is influenced by interface complementarity and the heme *b* redox potential, is very efficient with bimolecular rates between 2.9×10^5 and 1.1×10^6 M^{-1} s^{-1}.

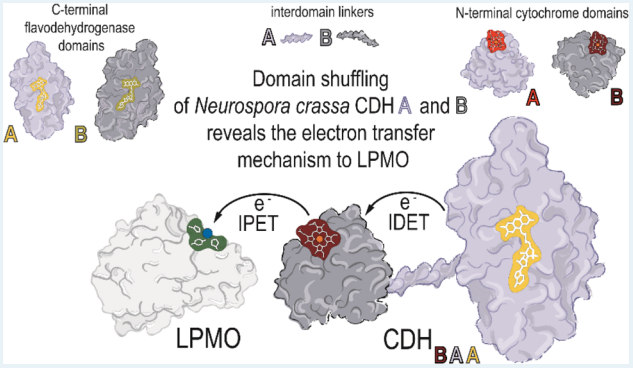

KEYWORDS: *cellobiose dehydrogenase, chimeric enzyme, domain swapping, electron transfer, lytic polysaccharide monooxygenase*

INTRODUCTION

The catalytic activity of lytic polysaccharide monooxygenase (LPMO) and its interaction with cellobiose dehydrogenase (CDH) have been reported to increase the rate of cellulose hydrolysis from the recalcitrant biomass and to increase the overall efficiency of enzymatic cocktails.[1−5] In contrast to electron-donating, low-molecular weight reductants of LPMO such as gallate or ascorbate, CDH is specific for LPMO and shows a fast electron transfer at physiological concentrations.[6,7] CDH is an extracellular flavocytochrome and contains FAD and a *b*-type heme in the flavodehydrogenase (DH) and cytochrome (CYT) domains, respectively, which are connected via a flexible linker. The electron transfer between the domains is pH dependent and has been studied by Igarashi and coworkers in detail.[8] Recently, the structure of the full-length protein has been elucidated and two conformations (closed- and open state) of the CYT domain were observed, which are supposed to play a role in interdomain electron transfer (IDET) and interprotein electron transfer (IPET).[9]

LPMO activation by CDH comprises three steps: (i) catalytic cellobiose oxidation in the DH active site leads to the formation of the reduced FAD cofactor, (ii) interaction of CYT with DH in the closed state results in the subsequent one-electron IDET, and (iii) interaction of CYT in the open state with LPMO results in the one-electron IPET. In the closed state of CDH, the FAD and heme *b* cofactors are in close proximity (~0.9 nm), which should favor IDET, whereas

Received: December 3, 2020
Revised: December 11, 2020
Published: December 24, 2020

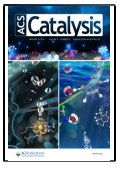

https://dx.doi.org/10.1021/acscatal.0c05294
ACS Catal. 2021, 11, 517−532

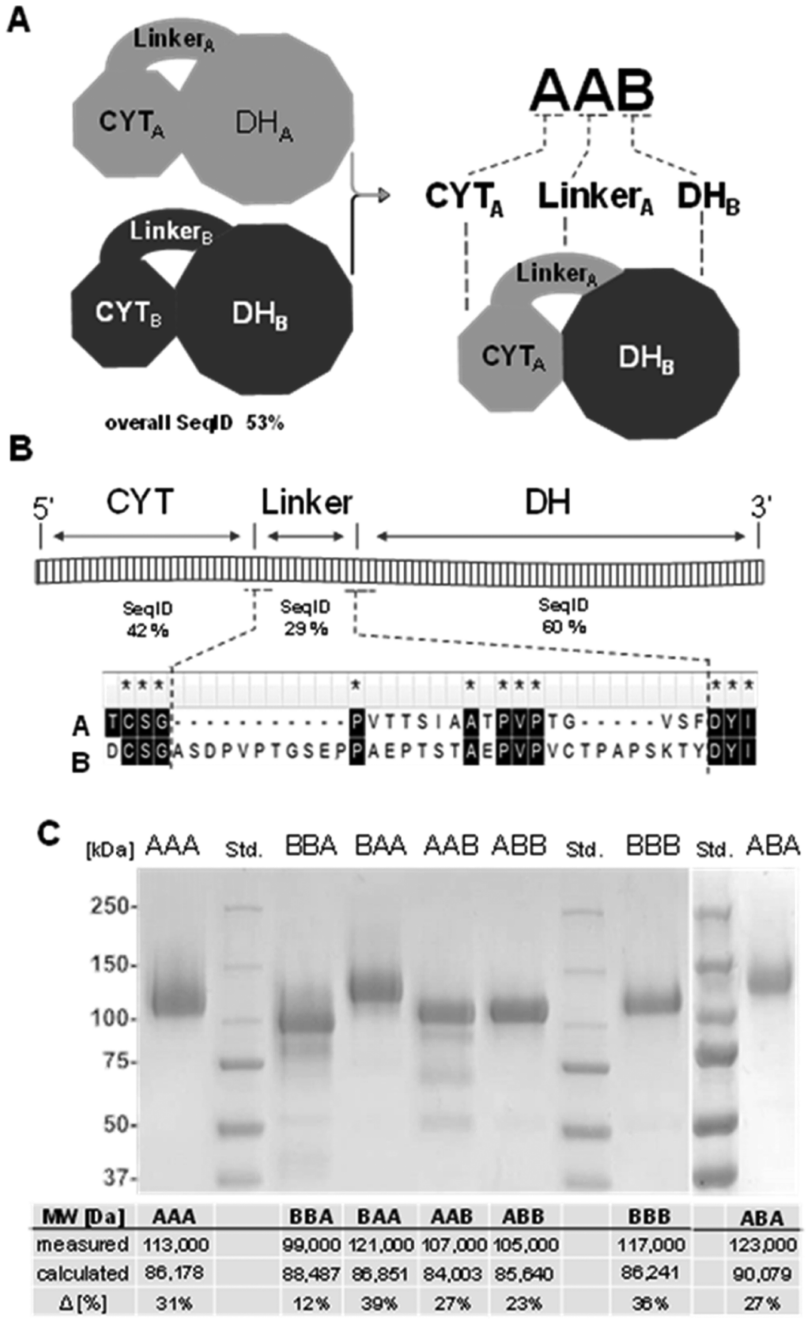

MW [Da]	AAA	BBA	BAA	AAB	ABB	BBB	ABA
measured	113,000	99,000	121,000	107,000	105,000	117,000	123,000
calculated	86,178	88,487	86,851	84,003	85,640	86,241	90,079
Δ [%]	31%	12%	39%	27%	23%	36%	27%

Figure 1. Properties of chimeric enzymes. (A) Domain architecture. The two *N. crassa* wild-type CDHs (CDHIIA denoted CDH_{AAA} and CDHIIB denoted CDH_{BBB}) consist of an N-terminal CYT domain, C-terminal DH domain, and a protein linker connecting the two domains. Four chimeric CDHs (CDH_{BBA}, CDH_{BAA}, CDH_{AAB}, and CDH_{ABB}) were created by domain swapping. (B) Linker sequence and position in CDH. The alignment shows sequence identities and the N- and C-terminal ends of the linkers. (C) Purified wild-type and chimeric CDHs. The measured and calculated molecular weights differ due to glycosylation.

IPET depends on the interaction of the heme *b* with LPMO,[9] which should be favored in the open state. The structure of the linker in the open- or closed states could not be fully determined in crystal structures, which indicates its high flexibility.

The two CDHs encoded in the genome of *Neurospora crassa* provide a good basis to study the influence of the CYT mobility on electron transfer because of several reasons. First, the structure of *Nc*CDHIIA has been elucidated (PDB ID: 4QI7), and second, a comparison of the steady-state kinetic constants of the two CDHs in a previous study found a 3.5-fold faster IDET rate for *Nc*CDHIIA at pH 6.0 compared to *Nc*CDHIIB despite the ∼50 mV higher redox potential of the heme *b* cofactor.[7] The independence of the IDET rate from the electrochemical driving force suggests a different function of both enzymes' CYT domains, possibly an adaptation to the copper center redox potentials of different LPMOs.[7] Structural features of the domains and surface charge distribution have been shown to influence the CDH domain interaction kinetics.[10,11] SAXS and SANS studies showed that the oxidized form of CDH populates a variety of conformational states between the closed- and fully open state and that pH, presence of divalent cations, and the presence of LPMO modulate the occupation of the closed- and open states.[12,13] Fast scanning

https://dx.doi.org/10.1021/acscatal.0c05294
ACS Catal. 2021, 11, 517−532

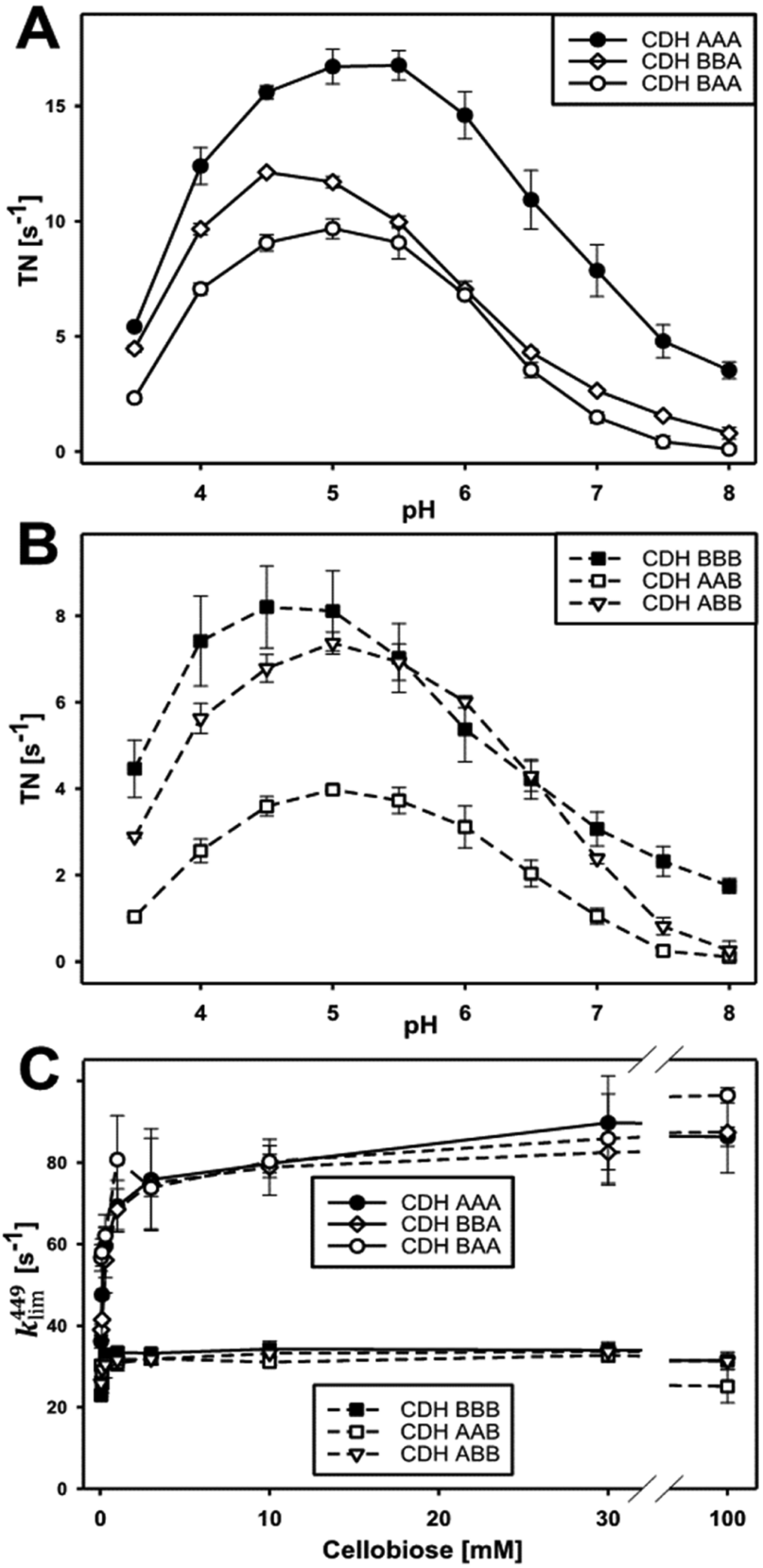

Figure 2. Effects of domain swapping on catalytic rates in the DH domain. (A) pH optima of cellobiose conversion in CDHs with a DH_A when using the two-electron acceptor 2,6-dichloroindophenol. (B) pH optima of CDHs with a DH_B using the same substrate and cosubstrate as in (A). (C) FAD reduction rate in all CDHs measured at 449 nm (k_{obs}^{449}) for increasing cellobiose concentrations.

AFM studies showed a preference of the open state in the reduced form of CDH.[14] These observations raise the question of how CYT interacts with either DH or LPMO and which structural and kinetic determinants govern this interaction.

https://dx.doi.org/10.1021/acscatal.0c05294
ACS Catal. 2021, 11, 517−532

Table 1. Catalytic Constants, Transient Rates, and FAD Redox Potentials of CDHs[a]

enzyme	k_{cat} [s^{-1}]	K_M [mM]	k_{cat}/K_M [M^{-1} s^{-1}]	k_{lim}^{449} [s^{-1}]	E vs SHE [mV]
CDH_{AAA}	17.8 ± 0.4	0.105 ± 0.003	1.7×10^5	81.8 ± 2.2	33 ± 5
CDH_{BAA}	9.0 ± 0.3	0.057 ± 0.006	1.6×10^5	82.2 ± 2.6	24 ± 5
CDH_{BBA}	14.2 ± 0.4	0.075 ± 0.005	1.9×10^5	79.8 ± 2.4	31 ± 1
CDH_{ABA}	9.1 ± 0.2	n.d.	n.d.	89.6 ± 2.3	n.d.
CDH_{BBB}	4.6 ± 0.1	0.027 ± 0.002	1.7×10^5	33.5 ± 0.4	43 ± 15
CDH_{ABB}	5.0 ± 0.1	0.026 ± 0.003	1.9×10^5	32.3 ± 0.4	33 ± 23
CDH_{AAB}	4.5 ± 0.2	0.046 ± 0.003	1.0×10^5	30.4 ± 0.6	n.d.

[a]The steady-state catalytic constants of the DH domains in wild-type and chimeric CDHs were determined for cellobiose as substrate and 2,6-dichloroindophenol as saturating co-substrate. Transient FAD reduction rates (k_{obs}^{449}) measured in a stopped-flow spectrophotometer at different cellobiose concentrations were used to extrapolate the maximal reduction rate of FAD for an infinite cellobiose concentration (k_{lim}^{449}). The midpoint redox potentials ($E^{1/2}$) of the FAD cofactor in regard to the SHE was determined in a spectroelectrochemical cell is given in the last column. All measurements were performed at pH 6.0. n.d.: not determined because of too small amount of chimeric CDH.

Based on sequence alignment and the elucidated crystal structures, we created chimeric CDH enzymes by exchanging linker, CYT, and DH domains of the two *Nc*CDHs to study the role of the CYT−DH interface, the effect of different cofactor redox potentials, and the influence of the linker length on the protein−protein interaction and IDET. CYT−LPMO interaction was also studied by hydrogen/deuterium exchange mass spectrometry (HDX-MS) measurements and transient-state kinetics to determine the interaction site of CDH−LPMO. We also evaluated the structural and kinetic determinants of the domain interaction to test recent results obtained by Courtade et al., who showed the binding of CDH and CYT to the LPMO active site by means of ^{15}N-HSQC and ^{13}C-aromatic-HSQC,[15] and by Laurent et al. who modeled the interaction between both enzymes.[16]

To study the effect of (i) the surface complementarity at the protein−protein interface, (ii) differences in the redox potentials of the cofactors, and (iii) the linker length on the domain interaction and the electron transfer rate, a domain swapping strategy was applied to create chimeric enzymes of the two *N. crassa* CDHs by exchanging CYT and linkers with different structural and physical properties. The chimeric CDHs were studied by steady-state and presteady-state kinetics, electrochemical methods, and molecular modeling in combination with two *N. crassa* LPMOs.

RESULTS

Construction and Properties of Chimeric CDH Variants. A domain swapping strategy was applied to exchange linkers and CYT domains of the two *N. crassa* CDHs (Figure 1A). The sequence alignment of *Nc*CDHIIA (UniProt: Q7RXM0) with *Nc*CDHIIB (UniProt: Q7S0Y1) gives a sequence identity of 53% and was used together with the crystal structure of *Nc*CDHIIA (PBD ID: 4QI7) and a homology model of *Nc*CDHIIB to define the individual CDH domains. The end of the N-terminal CYT domain is defined by a cysteine residue forming a disulfide bond (CYT_A: Q1−C211, CYT_B: Q1−C216, for brevity, we denote the domains and the linker of *Nc*CDHIIA by A and *Nc*CDHIIB by B). This disulfide bond in CYT is found in several CDHs and possibly evolved to stabilize the C-terminus against mechanical stress exerted by the linker. After this cysteine, the linker sequence starts ($linker_A$: S212−S229, $linker_B$: S217−T250). The DH domain starts with the first amino acid firmly connected with DH and ends with the C-terminus (DH_A: F230−V772, DH_B: Y251−R805). The C-terminus of *Nc*CDHIIA features an additional family 1 carbohydrate-binding module (CBM1, P773−V806), which is not present in *Nc*CDHIIB. Because in this study the binding of CDHs to cellulose is not interfering with the experiments, the CBM1 was not removed. It is present in all chimeric CDHs with a DH_A domain. The sequence identities of individual linkers, CYT and DH domains deviate considerably from the global sequence identity (Figure 1B). The catalytically active DH domains are most conserved, the linkers least. The linkers of both enzymes are rich in serine, threonine, and proline but differ substantially in length. $Linker_A$ consists of 17 amino acids, while $linker_B$ is twice as long and consists of 33 amino acids. The evolutionary divergence of the CYT domains and linkers points toward different mechanistic properties, physiological functions, and interacting LPMOs.

Production and Purification of Enzymes. Wild-type *N. crassa* CDHs (*Nc*CDHIIA denoted CDH_{AAA} and *Nc*CDHIIB denoted CDH_{BBB}) and five chimeric CDHs (CDH_{AAB}, CDH_{ABB}, CDH_{BBA}, CDH_{BAA}, and CDH_{ABA}) were recombinantly produced in *Pichia pastoris* and chromatographically purified (Figure S1 and Table S1). LPMO9C and LPMO9F from *N. crassa* were also produced in *P. pastoris* and chromatographically purified. The molecular weight of the individual domains and linkers can be calculated from the amino acid sequence and summed up to obtain molecular weights for full-length CDHs (Figure 1C). Similar molecular weights for the two wild-type enzymes CDH_{AAA} and CDH_{BBB} are predicted, and also between the smallest and largest chimeric enzymes (CDH_{AAB} and CDH_{BBA}, respectively) the mass difference is only 4484 Da. The molecular weights of the six purified CDHs determined by sodium dodecyl sulphate-polyacrylamide gel electrophoresis (SDS-PAGE) differ from the calculated values. The observed molecular weights are 12−39% larger and a result of posttranslational *N*-glycosylation[17] and *O*-glycosylation.[18] Considerable differences in the glycosylation, even between structurally quite similarly built chimeric CDH_{BBA} and CDH_{BAA}, point toward batch-to-batch variations between fermentations or differences in the post-translational processing of the chimeric CDHs. This heterogeneity of glycoforms is also known from homologously secreted CDHs and cannot be avoided so far. A deglycosylation of CDH results in low stability and solubility. The effects of differences in the *O*-glycosylation of the linker are unknown but might influence its flexibility. Bivariate correlation analysis of the mass percentage of each CDH's glycosylation shows no correlation with the domain composition in wild-type or chimeric CDH and also no correlation with the observed catalytic- or electron transfer rates later reported (Figure S7,

https://dx.doi.org/10.1021/acscatal.0c05294
ACS Catal. 2021, 11, 517−532

last column). The UV−visible (UV−vis) spectra of the oxidized and reduced chimeric CDHs reveal that the FAD and heme *b* cofactors are properly incorporated (Figure S2).

Catalytic Performance of DH Domains in Chimeric CDHs. In the reductive half-reaction, the oxidation of cellobiose in the active site of the DH domain results in the formation of cellobiono-δ-lactone and the reduced cofactor. In the oxidative half-reaction, the two electrons stored at the $FADH_2$ are then transferred to the heme *b* cofactor in the CYT domain in two separate, one-electron transfer steps to provide electrons for LPMO reduction.[7] Alternatively, the electrons can be transferred from $FADH_2$ to a two-electron acceptor such as 2,6-dichloroindophenol, which allows the assessment of catalysis without the contribution of the subsequent electron transfer step to the CYT domain. To investigate if the exchange of the CYT domain influences catalysis in the DH domain, we determined the pH optima, steady-state catalytic constants, and presteady-state rates for the two wild-type CDHs and the four chimeric CDHs.

The pH-dependence of the catalytic reaction with cellobiose and 2,6-dichloroindophenol resulted in bell-shaped pH profiles with optima between 4.5 and 5.5 (Figure 2A,B). In comparison with the wild-type enzymes, the chimeric CDHs show a slight shift of the pH optimum, narrower peaks, and a reduced activity above pH 7. The catalytic constants and presteady-state rates were determined at pH 6.0 (Figure 2C and Table 1). At this pH, the optimal CDH−LPMO interaction was observed,[6] which is important for IPET experiments. The determined K_M and k_{cat} of CDH_{AAA} for cellobiose are both about four times higher than that of CDH_{BBB}, which results in the same catalytic efficiency. In the presence of CYT_B, the K_M and k_{cat} of DH_A are slightly lower compared to CDH_{AAA}, whereas the presence of CYT_A has no significant effect on the K_M and k_{cat} of DH_B compared to CDH_{BBB}. Statistical analysis shows, as expected, a strong correlation between the type of the DH domain and the k_{cat} for cellobiose, whereas no correlation is found for the influence of the CYT domain on k_{cat} (Figure S7). The catalytic efficiencies at pH 6.0 are similar for all wild-type and chimeric CDHs, which renders this pH suitable for studying the subsequent IDET and IPET steps.

The presteady-state reduction rates of FAD at 449 nm (Figure 2C, k_{obs}^{449}) and the extrapolated limiting rates for infinite substrate concentrations (Table 1, k_{lim}^{449}) show that enzymes with a DH_A domain oxidized cellobiose ~2.5 times faster than enzymes with a DH_B domain but no influence of the swapped CYT domains is observed. A plot of the k_{obs}^{449} versus the cellobiose concentration indicates a higher substrate affinity of the DH_B active site, which is in agreement with the results from steady-state analysis. The performed experiments show that the reductive-half reaction of DH is not affected by a swap of the CYT domain. No bivariate correlation was found between CYT-type and k_{obs}^{449} in contrast to the high correlation between DH-type and k_{obs} (Figure S7).

Cofactor Redox Potentials in Chimeric CDH. The FAD and heme *b* cofactors in CDH make close contact (~0.9 nm edge-to-edge distance) in the enzyme's closed state. To determine if a domain swap influences the redox properties of FAD (Table 1) and heme *b* (Table 2), the midpoint redox potentials of the wild-type and chimeric CDHs were measured. However, no significant change was found. The midpoint redox potentials of FAD in all CDHs were between 24 and 43 mV versus standard hydrogen electrode (SHE). The spectroelectrochemical measurement of the relatively low FAD absorbance in the presence of the strong CYT Soret-band resulted in bigger errors for enzyme solutions with a lower enzyme concentration. The low amount of purified CDH_{AAB} and CDH_{ABA} did not allow the determination of its FAD redox potential. In contrast to the similar redox potential of FAD in DH_A and DH_B, the heme *b* redox potential in the CYT domains differ by about 60 mV. While CYT_A showed little modulation of its redox potential in wild-type and chimeric CDHs (~97−110 mV vs SHE), the CYT_B redox potentials were slightly increased (169 and 172 mV vs SHE) in the chimeric CDHs compared to wild-type CDH_{BBB} (158 mV vs SHE). However, statistical analysis shows no significant correlation between the type of the DH domain and the CYT midpoint potential (Figure S7).

Table 2. Steady-State and Transient-State IDET Rates and Heme *b* Redox Potentials[a]

enzyme	TN@pH 6 [s^{-1}]	IDET [s^{-1}]	*E* vs SHE [mV]
CDH_{AAA}	6.14 ± 0.12	50.00 ± 0.10	102 ± 4
CDH_{BAA}	0.50 ± 0.03	0.40 ± 0.02	172 ± 5
CDH_{BBA}	0.04 ± 0.01	0.02 ± 0.02	169 ± 5
CDH_{ABA}	2.05 ± 0.01	8.42 ± 0.23	110 ± 2
CDH_{BBB}	1.93 ± 0.03	4.00 ± 0.01	158 ± 2
CDH_{ABB}	0.48 ± 0.01	0.40 ± 0.01	97 ± 4
CDH_{AAB}	0.52 ± 0.01	0.40 ± 0.02	103 ± 4

[a]Comparison of cytochrome *c* reduction rates (turnover numbers, TN) as an indicator of IDET with transient rates (k_{obs}^{563}) at pH 6.0, along the heme *b* midpoint redox potentials (*E* vs SHE).

IDET in Chimeric CDHs. Cellobiose oxidation in the DH domain is followed by IDET from the $FADH_2$ or FAD semiquinone to the oxidized heme *b*. Steady-state kinetic measurements with cellobiose and the one-electron acceptor cytochrome *c*, which interacts only with CYT but not with the DH domain, were used to compare wild-type and chimeric CDHs (Figure 3A and Table 2). The cytochrome *c* turnover number (TN) of CDH_{AAA} was about 3.5-fold higher than that of CDH_{BBB}, which corresponds to the faster catalytic turnover found for DH_A. All chimeric CDHs exhibit lower cytochrome *c* TNs than the wild-type CDHs, but it is surprising that for four out of the five chimeric enzymes the decrease is only 3−12-fold. Only CDH_{BBA} showed an almost complete shutdown but still had a measurable IDET. This indicates two points: (i) the relatively good compatibility of the DH domains with unfamiliar CYT domains despite their low sequence identity of 42% and (ii) the influence of the linker on the CYT−DH interaction, which is demonstrated by the reduced IDET of chimeric CDHs featuring the longer $linker_B$. In CDH_{ABA}, the longer linker reduced the steady-state turnover of cytochrome *c* by a factor of 3 and the IDET rate by a factor of 19. The pH optimum of the IDET was partially influenced by the domain swapping. The wild-type CDH_{BBB} has a lower pH optimum (pH 4.5) than CDH_{AAA} (pH 5.5) but exhibits a plateau until pH 8.0. The pH optima of chimeric CDHs are identical or close to that of the respective DH domain, which can be explained by the isoelectric points of the individual domains. The CYT domains in CDH typically have a very low pI of ~3, whereas the DH domains have a pI of ~5.[19] The deprotonation of acidic amino acid residues on the DH domain close to the CYT−DH interface generates electrostatic repulsion of the strongly negatively charged CYT domain. Interestingly, the plateau observed for CDH_{BBB} is also found in CDH_{BBA} and CDH_{BAA} and thus seems to be a feature of CYT_B.

https://dx.doi.org/10.1021/acscatal.0c05294
ACS Catal. 2021, 11, 517−532

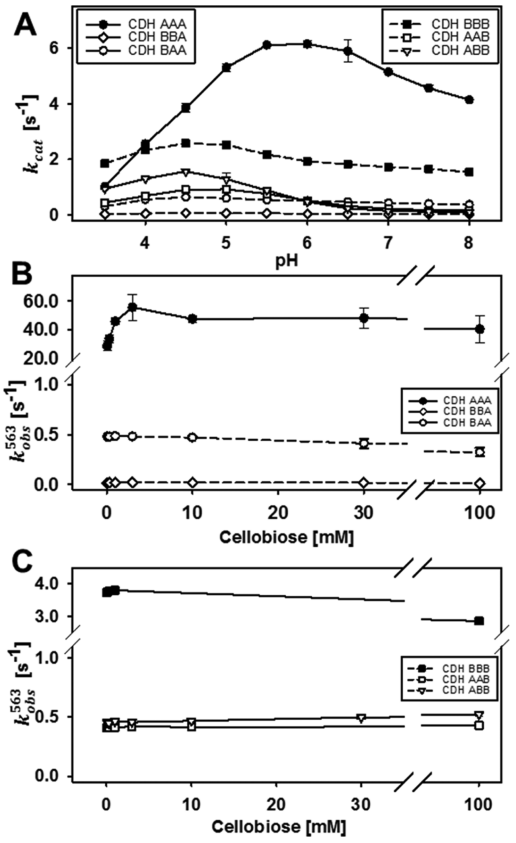

Figure 3. Effects of domain swapping on IDET. (A) pH optima of cytochrome *c* turnover numbers for wild-type and chimeric CDHs. (B) IDET rates (k_{obs}^{563}) of DH_A to different CYT domains measured for increasing cellobiose concentrations. (C) IDET rates of DH_B to different CYT domains measured for increasing cellobiose concentrations.

Although the IPET between CYT and cytochrome *c* is very fast,[20−22] it still could influence the observed IDET rate. Therefore, we also measured the transient reduction rate of the heme *b* cofactor to avoid a possible rate-limiting step. This direct measurement of IDET in CDH was performed by stopped-flow spectrophotometry at 563 nm to observe the reduction of the heme *b* α-peak (Figure 3B,C and Table 2). The observed transient rates are consistent with the trend of the steady-state rates with the wild-type CDHs having the most efficient IDET. The data also show that the cytochrome *c* assay provides a good estimate for the IDET rate in chimeric CDHs but not for the faster wild-type CDHs. As expected, the IDET rate (k_{obs}^{563}) of all CDHs is slower than the respective FAD reduction rates (k_{obs}^{449}). However, in the case of CDH_{AAA}, k_{obs}^{563} is 50 s^{-1} and very close to k_{obs}^{449} (80 s^{-1}). In this case, IDET is limited at low cellobiose concentrations (<1 mM). For CDH_{BBB} and all chimeric CDHs, a much slower IDET was observed and, therefore, a limitation was found only for substrate concentrations below 50 μM. Considering that the redox potential difference between CYT_A and DH_A (~102 mV) is lower than for CYT_B and DH_A or DH_B (~158 mV), the thermodynamic driving force between the cofactors is obviously irrelevant for the IDET rate. Also, no statistical correlation was observed between the midpoint redox potential and IDET rate (Figure S7). This exciting observation was further investigated by calculating the electron transfer rate based on the Marcus theory of electron tunneling. A modified version used by Dutton and coworkers[23,24] was applied using reported maximum, average, and minimum values for the quantum mechanical constants (λ, B, E) for the calculation of the corresponding distance-dependent electron transfer rates. The average edge-to-edge distance between the FAD and the heme *b* propionate A in docking models of CDH_{AAA} and CDH_{BBB} was found to be 0.9 nm, respectively (Figure 4). This corresponds to theoretical IDET rates in the order of 10^5 to 10^6 s^{-1}, which are at least four orders of magnitude faster than the measured IDET rates.

Considering the observed mobility of the linker and CYT domain in CDH, we postulate that this large difference between the calculated and the measured rates is because of conformational changes: the transition between the open- and

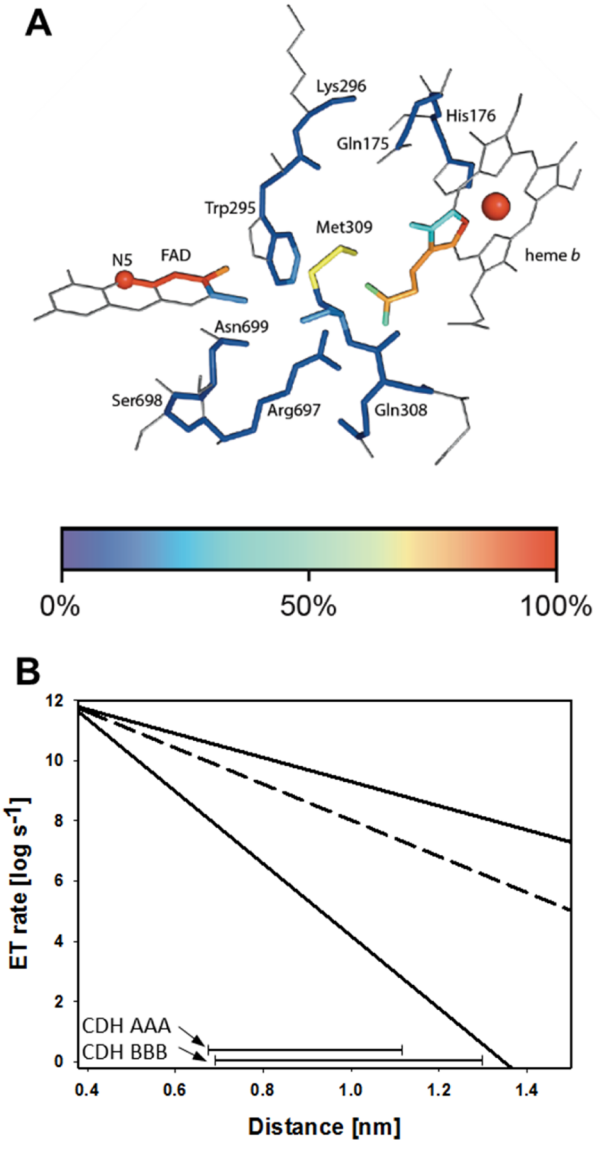

Figure 4. Electron transfer in CDH (IDET). (A) Detail of the crystal structure of *Mt*CDHIIA (PDB: 4QI6) featuring the closed-state conformation. The edge-to-edge distance between the FAD and heme cofactors is 0.9 nm. (B) Electron transfer rate plotted against cofactor distance for CDH (lower and upper limit, solid lines; most probable parameters, dashed line). The bars at the bottom indicate the observed IDET rates and edge-to-edge distances for CDH_{AAA} and CDH_{BBB} in docking calculations.

https://dx.doi.org/10.1021/acscatal.0c05294
ACS Catal. 2021, 11, 517−532

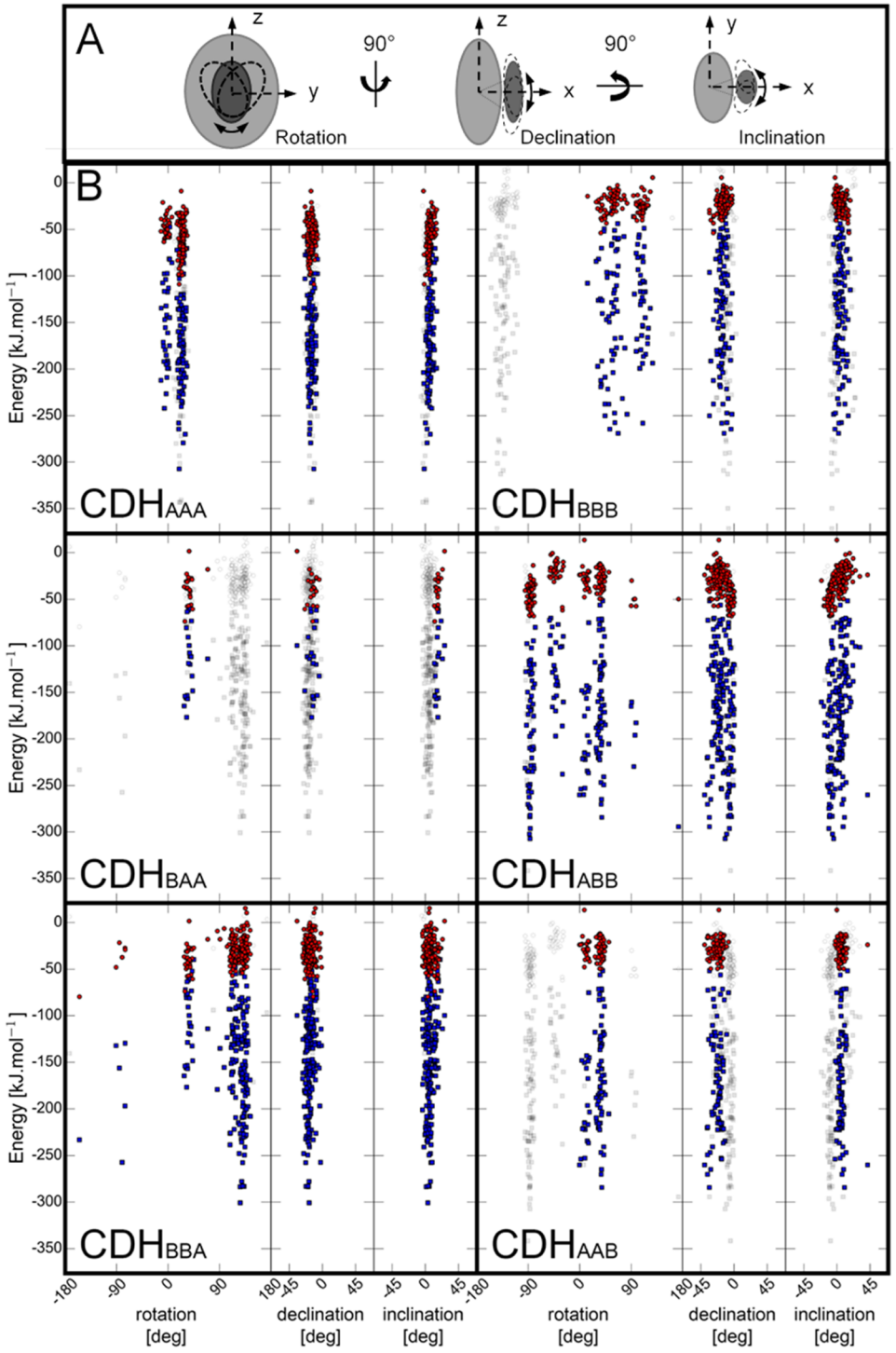

Figure 5. Orientation of CYT to DH in docking poses. (A) Schematic representation of evaluated angles. (B) From a total of 200 docking poses for each CYT−linker−DH pair the angle of rotation, declination, and inclination were measured in regard to its deviation from the crystal structure of the closed-state conformation of *M. thermophilum* CDH (PDB ID: 4QI6). The electrostatic (red) and van der Waals (blue) binding energies for each pose are given in kJ mol^{-1}. Docking poses in wild-type CDH_{AAA} and wild-type CDH_{BBB} are compared to docking poses of chimeric CDH_{BAA}, CDH_{ABB}, CDH_{BBA}, and CDH_{AAB}.

closed states of the CDH. The optimal, closest possible distance between the FAD and heme *b* cofactors depends on the correct orientation of the CYT domain at its DH domain interface. The open-state distance between the cofactors can easily exceed 1.5 nm and shut down IDET. With IDET depending on the closed state or at least very close proximity between DH and CYT, a steric mismatch between the domain surfaces, repulsive electrostatic interactions, or a linker that provides too much mobility will reduce IDET. This is supported by the inspection of the k_{obs}^{563} rates for both evolved wild-type CDHs and the chimeric CDHs (Table 2). The IDET for the constructed chimeric enzymes decreased by one order of magnitude for CDH_{AAB}, CDH_{ABB}, and CDH_{ABA}, two orders of magnitude for CDH_{BAA}, and three orders of

https://dx.doi.org/10.1021/acscatal.0c05294
ACS Catal. 2021, 11, 517−532

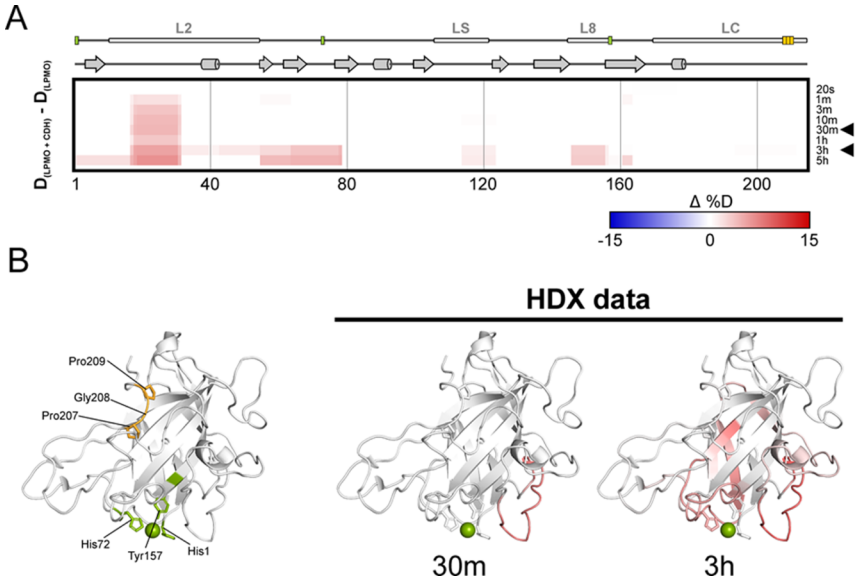

Figure 6. Structure dynamics arising from *N. crassa* LPMO9F and CDH_{AAA} interaction detected by H/D exchange. Structural differences between free LPMO and LPMO in the presence of CDH_{AAA} were visualized using a difference heat map (A) (http://peterslab.org/MSTools/). Deuteration levels of the protein alone were subtracted from those observed for the protein in the presence of CDH_{AAA}. Increased deuteration (deprotection) upon interaction is shown by red colors while protection is in blue (scale bar is at the bottom of the panel). Secondary structure elements, loops, and copper coordinating residues (green) and ProGlyPro patch (orange) are depicted above the heat map. Individual exchange times are shown on the right. Two selected time points (30 min and 3 h, indicated by arrowhead) were visualized on the LPMO structure (PDB ID: 4QI8) (B). The coloring scale follows the one in panel A. The central copper atom is shown in green and the side chains of the histidine brace residues and Pro-Gly-Pro patch are shown as sticks. The structure on the left visualizes histidine brace (green) and Pro-Gly-Pro patch (orange) residues.

magnitude for CDH_{BBA}. In the case of CDH_{ABA}, in which the CYT_A−DH_A interface is not altered, the longer linker results in an only 19 times lower IDET compared to the 125 times reduction of CDH_{BAA}, in which the CYT domain is swapped.

Based on the steady-state catalytic constants and k_{obs}^{563}, a limiting substrate concentration, above which the IDET confines the catalytic rate, can be calculated. For the naturally occurring *Nc*CDH_{AAA} and *Nc*CDH_{BBB}, already low cellobiose concentrations (55 and 35 μM, respectively) ensure that both CDHs reach their maximum IDET rate, which is the prerequisite of efficient LPMO reduction.

Evaluation of the DH−CYT Interaction Site by Docking. The program HADDOCK[25,26] was used to determine the interface of the four possible CYT−DH combinations found in the wild-type and chimeric enzymes by ambiguous restraint driven docking. A sample size of 200 docking poses for each CYT−DH pair was used for analysis. A "rotation" angle is used to define the rotation of CYT around a defined interdomain axis (Figure 5A and Table S2) in regard to DH, relative to the corresponding angle observed in the closed state of the *Myriococcum thermophilum* CDH structure (PDB ID: 4QI6). Similarly, we used the terms "declination" to describe the vertical offset angle and "inclination" to describe the horizontal offset angle of the docked CYT domain relative to the DH domain. The feasibility of docking poses was further assessed by considering the maximal extension of $linker_A$ and $linker_B$, which was estimated to be 6 and 11 nm, respectively. By using the distance field reaction coordinate as implemented in GROMOS++ software,[27,28] the shortest curved distance between the C-terminus of the CYT domain and the N-terminus of the DH domain not passing through the protein was computed. Docking poses, in which this distance was longer than the maximal extension of the linker, were excluded from subsequent analysis (Figure 5B, grey squares). The pH-dependent surface charges of the domains were calculated from pH 4−8 (Figure S3) and the protonation states corresponding to pH 6.0 were used for the docking. For this pH, the contribution of the van der Waals energy to the protein−protein interaction (−158.14 ± 62.2 kJ mol^{-1}) is generally 4−5 times higher than the electrostatic energy (−36.79 ± 20.9 kJ mol^{-1}), which indicates the importance of structurally complementary domain surfaces. A comparison of CDH_{AAA} and CDH_{BBB} shows that the declination and inclination angles of the 200 docking positions are narrower for CDH_{AAA}, which is indicative of a sterically more defined CYT−DH interaction. In CDH_{AAA}, the CYT rotation around the rotation axis is well defined by two groups with angles at −5 ± 15 and 25 ± 15°. The rotational position at 19.5° is preferred because it exhibits the strongest van der Waals and electrostatic interaction energies. In CDH_{BBB}, the docked rotational positions fall further apart (40 ± 50, 110 ± 20°), indicating a less directed interaction and a lower complementarity of the domain surfaces. The interaction energies are less favorable than in CDH_{AAA}. Interestingly, the energetically most favorable docking position of CYT and DH in CDH_{BBB} is not feasible because of the restricting length of the linker. This particular position with a rotation angle of −144.5° corresponds to an almost 180° rotation of the allowed rotational position with the second lowest van der Waals energy.

In chimeric CDHs, the linker plays an important role. The shorter $linker_A$ restricts the angular CYT orientation in CDH_{BAA} and CDH_{AAB} much more than the longer $linker_B$ in CDH_{BBA} and CDH_{ABB}. Only one angular orientation at 45 ± 25° is allowed by the length of $linker_A$, while the longer $linker_B$ allows for rotational positions between 45 ± 25 and 110 ± 40°. In the case of CDH_{BBA} (k_{obs}^{563} = 0.04 s^{-1}), the rotational orientation of CYT_B against DH_A at 126.3° is strongly preferred in terms of interaction energies (E_{vdW}: −300.7 kJ

https://dx.doi.org/10.1021/acscatal.0c05294
ACS Catal. 2021, 11, 517−532

mol^{-1}; E_{Elec} −40.4 kJ mol^{-1}) over rotational position at 32.7° (which is the IDET competent orientation in CDH_{BAA}), which has less favorable interaction energies (E_{vdW}: −176.8 kJ mol^{-1}; E_{Elec}: −22.8 kJ mol^{-1}). The steric restriction provided by $linker_A$ prevents the CYT in CDH_{BAA} to bind in a noncompetent position and thereby increases IDET (k_{obs}^{563} = 0.4 s^{-1}).

The average contact surface area for all possible complexes was calculated and averaged for each CYT−DH combination as well as the binding affinity using PRODIGY[29−31] (Table S3). The averaged contact surface areas correspond to ∼4% of the total DH surface area and ∼9% of the total CYT surface area. The small interaction site and low calculated affinities of the CYT−DH complexes (K_D = 3.2−47 μM) suggest a relatively transient and reversible interaction when compared to other redox proteins.[32]

Interaction Site of CYT with LPMO. Two interaction sites on CDH's CYT domain with LPMO have been proposed in the literature based on computational docking. One potential interaction site has been proposed to be opposite to LPMO's type-2 copper center around a conserved Pro-Gly-Pro patch,[33] which requires long-range electron transfer through LPMO but would allow the reduction of the substrate-bound LPMO. Another study suggested a direct interaction of heme *b* in CYT with the copper center of LPMO, which would necessitate the desorption of LPMO from its polymeric substrate. This mode would require no long-range electron transfer through the LPMO molecule.[9] To experimentally determine the protein−protein interaction site of CDH and LPMO in solution, H/D exchange kinetics were followed by mass spectrometry for CDH_{AAA} and *N. crassa* LPMO9F. This particular LPMO is well suited for such an analysis because it is relatively small (24.8 kDa) and lacks *N*-glycosylation, a C-terminal CBM1, and the linker region, which is often heavily *O*-glycosylated.[34]

Both proteins alone or in a mixture were subjected to H/D exchange followed by online digestion with pepsin and the resulting fragments were analyzed as described previously.[32] No detectable difference in the deuteration was observed on CDH_{AAA}. This could be caused by a combination of several factors: (i) a very short-lived or weak interaction of both enzymes, (ii) the protruding heme propionate-A group being the most prominent interaction partner leading to little involvement of other CYT residues, or (iii) the subsequent CYT−DH interaction interfering with the CYT deuteration.

For LPMO9F, on the other hand, protein backbone deprotection was observed in several peptide fragments when CDH was present in the solution. Visualization on the crystal structure (PDB ID: 4QI8)[9] shows that the perturbed protein regions occur in three loops surrounding the active site copper center (Figure 6). Although deprotection by the interaction is not the most common scenario in H/D exchange, it has been recognized as one of the possible biologically relevant outcomes.[35−37] In the case of CDH−LPMO interaction, it likely reflects the transient nature of the complex, where a short-lived interaction with the heme *b* in CYT leads to the local loosening of the structure around the copper center of LPMO and/or destabilization of the hydrogen bonding network in this region. Finally, no deuteration changes of any kind were observed around the conserved patch ^{207}Pro-Gly-Pro^{209} (Figure 6) close to the C-terminus.

Heterogenous Electron Transfer. CDH is recognized for its ability to directly transfer electrons to electrode surfaces via its CYT domain.[38] The heterogeneous electron transfer of wild-type and chimeric CDHs to a self-assembled monolayer (SAM) of thioglycerol on gold electrodes[7] was investigated for two reasons: (i) to verify that all produced enzymes and their domains are in their native, electron transfer competent conformation and (ii) to study the effect of swapped linkers and CYT domains on the direct electron transfer to an electrode. Unfortunately, CDH_{BBA} was not available in sufficient amounts for these experiments. In the presence of 20 mM cellobiose, catalytic currents were observed for all variants (Figure S4). The onset potentials of the anodic waves correlate well with the corresponding, spectroelectrochemically determined CYT redox potentials. Current densities were extracted at an overpotential of 200 mV, above the midpoint potential of the CYT domain (CYT_A at 300 mV, CYT_B at 360 mV vs SHE) and a scan rate of 15 mV s^{-1}. The highest current density was found for CDH_{AAA} (11.3 ± 1.8 μA cm^{-2}), followed by CDH_{ABB} (3.7 ± 1.5 μA cm^{-2}), CDH_{BBB} (2.6 ± 1.7 μA cm^{-2}), $CDHB_{BAA}$ (1.9 ± 0.3 μA cm^{-2}), and CDH_{AAB} (1.2 ± 1.0 μA cm^{-2}). Every CDH clearly showed direct electron transfer to the electrode and thereby verified the integrity of the electron transfer route.

Anodic and cathodic peak currents were obtained for all CDHs over a range of scan rates (3−150 mV s^{-1}). The plot of the peak currents versus the square root of the scan rates is linear for all enzymes and indicate a freely diffusing redox species and no adsorption onto the electrode (Figure S5). The peak separation of the anodic and cathodic peak increased with increasing scan rates (Figure S6). The heterogeneous electron transfer is reversible at very low scan rates and quasi-reversible at scan rates above 5 mV s^{-1}, pointing toward a fast electron transfer compared to mass transport. This allows the calculation of the heterogeneous electron transfer constant (k^0) according to the method of Nicholson and Shain for the quasi-reversible electron transfer regime.[39] All wild-type and chimeric CDHs show a similar k^0 between 7.7 and 17.7 × 10^{-4} cm s^{-1} at the most relevant scan speed for comparison (50 mV s^{-1}, Figure 7), which demonstrates that there is no restrained interaction of any CYT with the thioglycerol monolayer on the gold electrode and all CDH variants are functional. This is

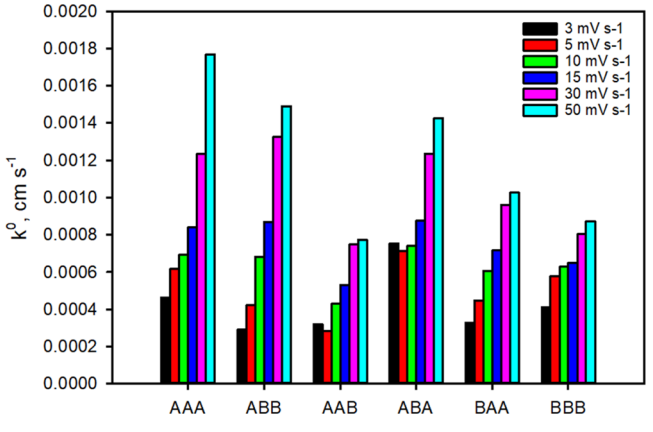

Figure 7. Heterogeneous electron transfer rates (k^0). k^0 was calculated from the peak separation of the anodic and cathodic wave observed from cyclic voltammograms measured at different scan rates (3−50 mV s^{-1}) according to Nicholson−Shain. Data from scan rates above 50 mV s^{-1} could not be used because the increased capacitive current did not allow the exact determination of the peak maxima. The data (peak separation vs scan rate) are given in Figure S6.

https://dx.doi.org/10.1021/acscatal.0c05294
ACS Catal. 2021, 11, 517−532

comparable with a k^0 of ca. 10^{-3} to 10^{-4} cm s^{-1} for cytochrome *c* on gold electrodes.[40] CDH_{BBB} with the lowest k^0 has the least efficient electron transfer of its CYT domain with the electrode.

IPET Kinetics. After verifying that the wild-type and chimeric CDHs are all electron transfer competent, we investigated the final electron transfer from CYT to LPMO (IPET). In sequential stopped-flow experiments, CDHs were prereduced by a stoichiometric amount of cellobiose. After 90 s in the aging loop, oxygen had fully reoxidized the $FADH_2$, which was necessary to prevent any interfering IDET to CYT. Then, the CDH with the reduced CYT was shot against an equimolar, 3-, 10-, and a 50-fold molar ratio of *Nc*LPMO9C to measure the IPET rate. A linear dependence of k_{obs}^{563} on LPMO concentrations was found (Figure 8), which indicates

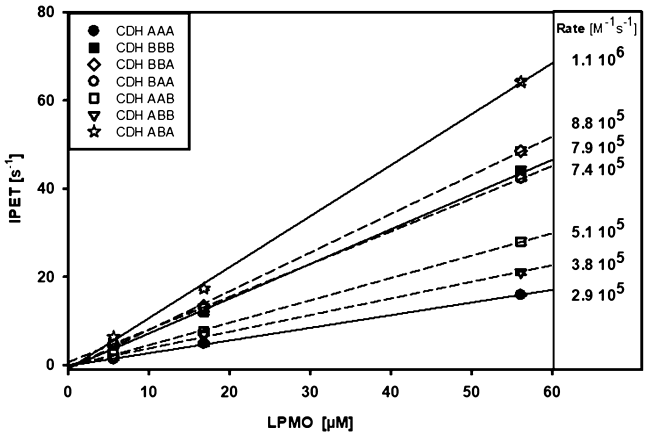

Figure 8. Effects of domain swapping on IPET. Stopped-flow measurements of the electron transfer from prereduced CYT to LPMO at 563 nm at for increasing LPMO concentrations show a linear relation from which bimolecular rates were calculated.

that the electron transfer between both enzymes is fast enough to show no saturation even for the highest measured LPMO concentration.[21] The bimolecular IPET rate was calculated from the slope of k_{obs}^{563} versus the LPMO concentration. The determined rates are all within the same order of magnitude, which indicates that the interaction mechanism is not evolved to recognize and favor specific CDH−LPMO combinations but is based on a universal recognition mechanism which depends little on surface complementarity. The observed differences in IPET show that CYT_B, which is present in three measured CDHs, exhibit a two times faster bimolecular rate with *Nc*LPMO9C (7.4−8.8 × 10^5 M^{-1} s^{-1}) than most CDHs with CYT_A (2.9−5.1 × 10^5 M^{-1} s^{-1}) with the exception of CDH_{ABA}, which exhibits the highest IPET rate. This points toward the importance of the linker and its influence on the closed- and open-state conformation. CDH_{AAA} with the short linker, the fastest IDET, and the slowest IPET prefers the closed-state conformation, whereas CDH_{BBA} or CDH_{ABA} with reduced IDET and fast IPET prefer the open-state conformation.

In contrast, a higher redox potential difference between the CDH and LPMO cofactors has not the expected, rate enhancing effect on the IPET rate (Table 2, Figure 8). CYT_B with its ∼60 mV higher midpoint potential compared to CYT_A has a comparatively lower driving force for electron transfer between the heme *b* and LPMO's type-2 copper but shows similar IPET rates to CYT_A. This indicates that CYT−DH combinations of poor surface complementarity or with an unsuitable linker preferably populate the IPET competent open-state conformation. We conclude that the closed- and open-state distribution of CDH populations define the electron transfer rates of CYT in IDET and IPET.

Multivariate Analysis. Mixed factor principal component analysis (PCA), including the quantitative variables (k_{cat}, k_{obs}, IDET, IPET, CYT midpoint redox potential, and glycosylation) and qualitative variables [DH-, CYT-, and linker-type (Tables S5 and Figure S9)], has been performed on the data set from wild-type and chimeric CDHs to explore intercorrelation. Glycosylation shows the smallest effect of all quantitative variables, while the kinetic variables cluster as expected from bivariate analysis.

DISCUSSION

The two-domain structure of CDH has been recognized soon after its discovery, by observing the spectral features of its two cofactors, proteolytic cleavage into the separated domains, and distinct catalytic properties of the full-length CDH and its DH domain. The domain organization became evident with the first isolated CDH sequence of *Phanerochaete chrysosporium*,[41] but the purpose of the CYT domain remained unknown. Crystallization experiments in which only the separated, proteolytically generated CYT and DH domains formed crystals indicated the high mobility of the linker and CYT domain.[18,42] At the same time, Igarashi et al. investigated the pH dependence of the IDET between the DH and CYT domains of *P. chrysosporium* CDH in a presteady-state kinetic study. He also determined the redox potentials of the heme *b* and FAD cofactor, which can influence IDET.[10]

However, the physiological function of the CYT domain and the highly variable length of the linker in CDHs (16−40 amino acids) remained enigmatic. Also, the considerable length of $linker_B$ in comparison to other flavocytochromes, for example, the flavocytochrome b_2's hinge (linker) region consisting of only 15 amino acids,[43] is unusual. In the two CDHs from *N. crassa*, $linker_B$ is almost twice as long as $linker_A$. Both enzymes have the lowest sequence identity (29%) among CDH's structural elements despite sharing two common features: a high percentage of serine, threonine, and proline residues and a conserved Pro-Val-Pro motif. Likewise, the sequence identity among the CYT domains (43%) is low compared to that of the DH domains (60%). The higher diversity of the linker and CYT sequences is observed for all CDHs and suggests an evolutionary adaptation to contact various redox partner proteins, while the DH domain serves as a source of electrons.

With the discovery of LPMO in 2010,[44] the physiological redox partner of CDH was finally revealed, which gives us the opportunity to study the CYT domain's IDET and IPET mechanism as part of a natural, extracellular electron transfer chain. This framework allows the testing of hypotheses on CDH's molecular, catalytic, and electron transfer properties. Swapping domains between the structurally, catalytically and electrochemically different CDHs of one organism allows differentiating between the functions of the involved domains and linkers in the electron transfer route from CDH's $FADH_2$ to LPMO's type-2 copper center. Two wild-type and five chimeric CDHs could be recombinantly expressed in *P. pastoris* and all enzymes except CDH_{AAB} and CDH_{BBA} could be produced in quantities above 10 mg, sufficient for a full set of analysis. The specific activities of the purified chimeric enzymes and their absorption spectra are in consonance with

https://dx.doi.org/10.1021/acscatal.0c05294
ACS Catal. 2021, 11, 517−532

the wild-type CDHs and, therefore, these enzymes are properly folded. However, a difference in the extent of glycosylation of the wild-type and chimeric CDHs was found. This variation is inevitable with the chosen yeast expression system, which is known to produce various glycoforms. However, the *N*-glycosylation sites are not located at the DH−CYT interface and thus should not affect the experiments. *O*-Glycosylation of the linker was previously reported,[45] but we lacked the resources to determine if this minor fraction of glycosides varied between the produced CDHs. However, the determined heterogeneous electron transfer rates for all CDHs were relatively similar and indicated no significant influence of the glycosylation on the interaction with the thioglycerol-modified gold electrode.

Transient kinetic studies of the catalytic reaction of the DH domain showed no change of the reductive half-reaction in chimeric CDHs but showed an effect of the swapped CYT domains on the oxidative half-reaction by shifting the pH optima for the two-electron acceptor 2,6-dichloroindophenol. The pH optima of CDH_{AAA} and CDH_{BBB} are identical to previous data.[7] Because the pH optimum of the catalytic reaction in CDH generally depends on the electron acceptor,[19,46] this indicates an impact of the CYT domain on the oxidative catalytic half-reaction. These results support the previously observed effect of the CYT domain on the catalytic step in the DH domain of *Crassicarpon hotsonii* (syn. *M. thermophilum*) CDH.[11] At pH 6.0, which is also the pH optimum of the CDH−LPMO interaction,[6] only small differences between the catalytic efficiencies were observed between the wild-type and chimeric CDHs, rendering this pH as suitable to study the subsequent electron transfer steps. The presteady-state reduction rates of FAD by cellobiose at 449 nm (k_{obs}^{449}) show a clear separation between enzymes with a DH_A domain (80−89 s^{-1}) and a DH_B domain (30−33 s^{-1}) but no effect of a CYT swap on the rate of the reductive-half reaction.

While the effects of the domain swap on the catalysis of the chimeric enzymes were moderate, the IDET between DH and CYT was strongly affected. Steady-state experiments showed different pH optima and 3−12 times (except for CDH_{BBA}) reduced TN's of the chimeric CDHs with cytochrome *c*. These findings were corroborated by transient-state data. The highest IDET rates were measured for wild-type enzymes, which had a 19 times (CDH_{AAA}) or 10 times (CDH_{BBB}) higher IDET rate than the successive chimeric CDHs. Modeling studies showed the importance of surface complementarity and the degree of orientational freedom provided by the linker. Given the varying length of $linker_A$ (7 nm) and $linker_B$ (11 nm), it can be expected that in the open state the distance limit for a reasonable fast electron transfer (∼1.5 nm) between CYT and DH is often exceeded. It was also found that the redox potential difference between CYT and DH is not the dominant driving force for IDET because CDHs with a CYT_A have a lower ΔE (64−104 mV) between the cofactors than CYT_B carrying CDHs (158−172 mV) but similar or faster IDET rates. The reason is the close edge-to-edge distance between the FAD and heme. For the typical distance of ∼0.9 nm in *N. crassa* CDH's closed state, the electron transfer rates are 10^5 times higher than the measured rates. This suggests that the mobility of the CYT domain and its shift between closed- and open-state conformations is the rate-limiting factor of IDET, rather than the electron transfer event itself. A shorter linker ($linker_A$) and a higher complementarity at the CYT−DH interface increases IDET by supporting the closed state of the CDH.

The efficiency of the subsequent electron transfer step from CYT to LPMO, the IPET, is most important for the efficiency of the process and determines the rate of LPMO reduction. A specific and fast IPET saves valuable resources for the metabolism of the cellulolytic organism (less enzymatic consumption of cellobiose, less secreted CDH needed) and prevents futile electron transfer to other electron acceptors or scavengers, which reduces not only the efficiency of the extracellular electron transfer system but could also produce degradation products detrimental to the organism's growth. The HDX-MS experiments showed the interaction of CYT and LPMO to happen via direct contact between their active centers. This is in agreement with NMR and docking studies.[15,16] No alternative interaction site of CYT−LPMO has experimentally found so far. The reported electron transfer between the active site copper and amino acids within LPMO resulting in tyrosyl- or tryptophanyl radicals indicates the presence of electron transfer pathways, which have been attributed to the protection of the active site during uncoupled turnover.[47,48] The observed interaction is relatively weak, underlining the formation of a flexible and transient complex. This observation aligns well with the necessity of the LPMO to detach from the cellulose in order to receive an electron from CDH, which fits very well to the proposed peroxide-dependent catalytic mechanism of LPMO.[49] The apparent transient interaction also complements previous findings,[45] hinting at a very dynamic system which depends on the interplay between electrostatic forces of its cofactors and thermodynamic forces governing domain movements.

The measured IPET rates all have the same order of magnitude, which indicates that the interaction mechanism did not evolve to recognize and favor specific CDH−LPMO combinations but is based on a universal recognition mechanism between the heme *b* propionate A and the copper center, which depends little on surface complementarity.[16] This is corroborated by reports on the interaction of different CDHs and LPMOs from *N. crassa*,[6] CDH and LPMO from different fungi[1,2,50] and even from fungal CDH to bacterial LPMOs.[51] The measured bimolecular rates for the final electron transfer step from CYT to LPMO were found to be very fast with values between 2.9×10^5 and 1.1×10^6 M^{-1} s^{-1}. A similar rate was also found for the very fast CYT−cytochrome *c* interaction (10^6 M^{-1} s^{-1}).[21] We conclude that the rate-determining driving force for IPET is not the redox potential difference between LPMO and CYT because CDHs with a CYT_B have a lower redox potential difference to LPMO but exhibit, in most cases, slightly faster IPET rates than CYT_A featuring CDHs. Likewise, the IPET rates do not show a preferred complementarity of either the CYT_A or CYT_B surface with *Nc*LPMO9C. This supports the previously published modeling of the CYT−LPMO interface, which shows that only a very small surface area of the domains besides the cofactors is involved in the recognition and interaction.[16] Hence, the most important factor for the higher IPET rates of chimeric CDHs over the wild-type CDHs seems to stem from their preference of the open-state conformation induced by an unfitting CYT−DH interface or linker.

EXPERIMENTAL PROCEDURES

Molecular Biology, Expression, and Purification. Genetic constructs of *cdhIIA* (NCU00206) and *cdhIIB*

https://dx.doi.org/10.1021/acscatal.0c05294
ACS Catal. 2021, 11, 517−532

(NCU05923) were described previously[7] and used for this study. A silent mutation (C456T) was introduced to the gene NCU05923 to delete the BstBI (Bsp119I) restriction site. Alignments using MEGA 6[52] applying the BLOSSOM 62 algorithm together with the 3D structure analysis of NCU00206 (PDB ID: 4QI7) were applied to define exact borders of the individual domains (Table S4). Fragments of the individual domains were generated and joined to create four chimeric constructs by overlap extension PCR. The genetic integrity of the amplicons encoding chimeric CDHs was checked by DNA sequencing at Microsynth (Wolfurt, Austria). Following established methods,[53] the constructs were expressed in a *P. pastoris* expression system (KM71H, Invitrogen). Best producing variants were preselected,[54] cultivated in 500 mL scale fermentations (Figure S1), and purified by hydrophobic interaction (PHE-Sepharose Fast Flow, GE Healthcare) and anion exchange chromatography (Source 15Q, GE Healthcare). Two chimeric CDHs (CDH_{AAB} and CDH_{BBA}) still contained minor impurities after these two steps and were subjected to additional size exclusion chromatography (Superdex 75). The SDS-PAGE analysis of all preparations used in this study is displayed in Figure 1.

Enzyme Activity Assays and Protein Quantitation. The activity of CDHs was determined in 1 mL assays by following the reduction of either 0.3 mM 2,6-dichloroindophenol (DCIP, ε_{520} = 6.8 mM^{-1} cm^{-1}) or 50 μM cytochrome *c* from equine heart (ε_{550} = 19.6 mM^{-1} cm^{-1}). Assays were buffered with 100 mM sodium citrate-phosphate buffer according to ref 55 at the indicated pH. The pH-dependent activity was measured with 30 mM lactose as saturating substrate. Assay reactions were monitored for 180 s at 30 °C at the indicated wavelengths in a LAMBDA 35 UV−vis spectrophotometer equipped with a temperature-controlled 8-cell changer (PerkinElmer). The protein concentration of wild-type and chimeric CDHs was determined via the absorbance at 280 nm and the theoretical molar absorption coefficient ε_{280} calculated with the Expasy Prot-Param program[56] using the mature amino acid sequence.

Spectroelectrochemistry. Spectroelectrochemical experiments were performed using 500 μL samples containing around 50 μM wild-type or chimeric CDH, 100 mM KCl, 100 mM potassium phosphate buffer pH 6.0, and a redox mediator mixture comprising anthraquinone-1,5-disulfonate, 2-hydroxy-1,4-naphthoquinone, indigo carmine, indigo trisulfonate, duroquinone, methylene blue, phenazine methosulfate, 1,2-naphthoquinone and *N,N,N′,N′*-tetramethyl-*p*-phenylenediamine (all 3 μM), and methyl viologen (150 μM). All experiments were carried out under anaerobic conditions at 25 °C in a thin-layer (*d* = 0.05 mm) spectroelectrochemical cell (BASi, West Lafayette, IN; USA) with a standard three-electrode setup comprising a AglAgCl—reference electrode (BASi), a platinum gauze (Goodfellow Cambridge Ltd., Huntington, England, UK) as the working electrode, and a platinum wire (Goodfellow Cambridge Ltd.) as the auxiliary electrode. Potentials were applied using a Gamry Series G 300 Potentiostat/Galvanostat/ZRA (Gamry Instruments, Warminster, PA, USA). A Whitley DG 250 Anaerobic Workstation (Don Whitley Scientific Ltd., Shipley, England, UK) was used to work under oxygen-free conditions. The reference electrode was calibrated against a saturated calomel electrode. All potentials are reported relative to the SHE. Nernst plots consisted of at least 5 data points, showed linear behavior, and were consistent with a one-electron redox process in the case of the heme *b* and a two-electron process in the case of the FAD.

Voltammetry. Preparation of enzyme-modified electrodes started with the cleaning of gold disk-electrodes (*d* = 1.6 mm, BASi, West Lafayette, IN, USA) by dipping in acidic piranha solution [H_2SO_4/H_2O_2 = 3:1 (v/v)] for 5 min, cycling in 0.1 M NaOH (−0.205 to −1.205 V vs AglAgCl, 10 cycles, 100 mV s^{-1}), polishing to mirror finish with aqueous alumina particles (0.05 μm) on a MicroCloth (Buehler, Lake Bluff, IL, USA), ultrasonication to remove residual polishing particles and cycling in 0.5 M H_2SO_4 (−0.205 to +1.705 V vs AglAgCl, 20 cycles, 200 mV s^{-1}). After rinsing with ultrapure water and drying with nitrogen gas the electrodes were immersed overnight in 10 mM 1-thioglycerol dissolved in absolute ethanol for SAM formation. The electrodes were then washed with 20% ethanol to remove unbound thioglycerol, ultrapure water and dried over a stream of nitrogen gas. A custom-made Teflon holder was put over the electrode surface, leaving a cylindrical cavity with a volume of ∼20 μL above the thioglycerol-modified gold surface. Then, a 100 μM CDH solution in 100 mM McIlvaine buffer, pH 6.0, was applied to the cavity. The assembly was covered with a dialysis membrane (45 kDa cut-off) held in place via a rubber O-ring.

Electrochemical experiments were carried out using a PGSTAT204 potentiostat/galvanostat (Metrohm Inula GmbH, Vienna, Austria) with a standard three-electrode setup comprising the enzyme-modified gold electrode as working electrode, a platinum wire as the counter electrode, and a AglAgCl electrode as the reference electrode. The 100 mM McIlvaine buffer, pH 6.0 contained 0.1 M KCl as the supporting electrolyte. A typical set of experiments comprised cyclic voltammetry of the thioglycerol-modified electrode (blank), the enzyme-modified thioglycerol-electrode, the enzyme-modified thioglycerol-electrode in the presence of 20 mM cellobiose, and the enzyme-modified thioglycerol-electrode in the presence of 20 mM cellobiose and 50 μM ferrocenemethanol. The applied potential window ranged from 5 to 550 mV versus SHE. Scan rates were varied from 3 to 500 mV s^{-1}. Before the start of the experiment, the electrochemical cell containing buffer and the electrode setup was deoxygenated by purging with argon gas for 15 min. The bulk solution was not agitated during the measurement which was performed at 25 °C.

Cyclic voltammograms were analyzed using NOVA software (Metrohm) and Microsoft Excel. To evaluate whether freely diffusing or adsorbed CDH species dominate the electrochemical process, the linearity of plots of peak current versus the square root of the scan rate was analyzed. Reversibility, quasi-reversibility, or irreversibility of the electron transfer process was assessed by the shape of the voltammograms and the peak-to-peak separation. Standard heterogeneous electron transfer rate constants k^0 were calculated using the model for quasi-reversible processes described by Nicholson & Shain[57] and Matsuda & Ayabe[58] with a transfer coefficient of α = 0.5 and interpolated values [$\Psi = 1/(-2.46 + 0.041)*dE_p$] of the kinetic parameter Ψ for the scan rate-dependent peak potential separation. Diffusion coefficients for CDH were calculated from the slope of the linear correlation of the anodic or cathodic peak currents, the square root of the scan rate, the active electrode surface area (A = 0.0177 cm^2), and an enzyme concentration of 100 μM (10^{-7} mol cm^{-3}) applying the Randles−Sevcik equation.[59,60] Peak currents were assessed by

https://dx.doi.org/10.1021/acscatal.0c05294
ACS Catal. 2021, 11, 517−532

applying Nicholson's empiric equation $I_{pa}/I_{pc} = (I_{pa})_0/I_{pc} + 0.485(I_{sp})_0/Ipc + 0.086$.[39]

Presteady-State Kinetic Studies. The rapid spectral changes induced by substrate oxidation and the resulting change of the redox state of the CDH cofactors were followed with a SX-20 stopped-flow instrument (Applied Photophysics, Leatherhead, UK) equipped with a photomultiplier tube (AP/PMT.R928). The redox state of the FAD cofactor was monitored at the appropriate isosbestic point (449 nm) of the heme *b* cofactor, which itself was monitored at 563 nm. The observed rates (k_{obs}) for the indicated cellobiose concentrations were estimated by fitting the data to a single exponential function. The reduction of *Nc*LPMO9C by CDH was studied using a UV−vis photodiode array detector (AP/SXPDAUV) in the sequential mixing mode. CDH was fully reduced in the first step by mixing with an appropriate concentration of cellobiose in air-saturated buffer. The reaction was held in an ageing loop until full reoxidation of the FAD cofactor occurred via its weak oxidase activity. Approx. 70% of the heme *b* remained reduced because of its slower interaction with O_2. The partially reoxidized CDH was rapidly mixed with *Nc*LPMO9C. The observed rates of transfer were estimated by following the redox state of the CYT domain of CDH and fitting the data of A_{563} to a single exponential curve. All presteady-state experiments were performed in 100 mM sodium citrate-phosphate buffer, pH 6.0 at 30 °C.

Modeling of CDH Chimeras. SWISS-MODEL[61−63] was used to generate structure-guided homology models of the CYT and dehydrogenase (DH) domains of *Nc*CDHIIB (ORF: NCU05923) using the crystal structure of *Nc*CDHIIA (PDB ID: 4QI7)[9] as a template. Steepest descent energy minimization with 2500 steps (initial step size of 0.1 nm) was performed with the GROMOS software package for molecular simulation[64] using the 54a7 force field[65,66] as a further refinement for the resulting homology models. Subsequently, the complexes CYT_A−DH_A, CYT_A−DH_B, CYT_B−DH_A, and CYT_B−DH_B have been modeled using HADDOCK 2.2[25,26] with interaction restraints between heme *b* and the Arg697 and Arg719 for *Nc*CDHIIA and *Nc*CDHIIB, respectively. The number of starting structures was set to 1000 and refined to 200 structures. Nonbonded energy values (i.e., van der Waals and electrostatic energies) were taken from the HADDOCK output and the angles of the CYT domain relative to the DH domain around three axes defined by two (virtual) atoms j and k was measured by computing the dihedral angle *i*−*j*−*k*−*l* with the (virtual) atoms, as listed in Table S2. The distance-field reaction coordinate[28] was used to estimate the shortest distance between the linker anchor points along a path that does not pass through the protein domains. Electrostatic surface representations, as well as protonation states, were computed with PROPKA 3.1,[67,68] PDB2PQR[69] and the PyMOL APBS plug-in.[70−74] Binding affinities were predicted with PRODIGY.[75−77]

H/D Exchange Mass Spectrometry. Prior to the mass spectrometric analyses, *Nc*CDHIIA was deglycosylated under nondenaturing conditions as utilized previously for the analyses of CDH from *M. thermophilum*.[35] CDH was incubated overnight with 15 U Endo Hf (New England Biolabs, USA) per 1 μg of protein at 37 °C in 50 mM sodium acetate buffer pH 5.75 to detach the *N*-glycans. The deglycosylated CDH was preincubated alone or in a mixture with *Nc*LPMO9F (1:3 and 3:1 M ratios) in H_2O-based 50 mM sodium acetate buffer pH 5.75 for 30 min. After preincubation, the deuterium labeling was started by a 10-fold dilution of the protein samples into a deuterated buffer (50 mM sodium acetate pD 5.75). The final protein concentration during the labeling was 5 μM for the examined protein and 15 μM for the interaction partner. The deuteration reaction proceeded at 21 °C and 50 μL aliquots were removed after 0.33, 1, 3, 10, 30, 60, 180, and 300 min. The rest of the HDX-MS workflow, including the stopping of the exchange in the aliquots, denaturation of samples, and their online enzymatic digestion by immobilized porcine pepsin, LC−MS analysis by Fourier transform ion cyclotron resonance mass spectrometry and data processing, was performed exactly as optimized for *M. thermophilum* CDH as described elsewhere.[35]

Statistical Analysis. A statistical evaluation of the data set, which aimed to identify significant correlations of individual variables using bivariate correlation analysis and PCA has been performed using the software R Studio (MA, USA) and the packages FactoMiner[78] and Psych.[79] Selected code snippets describing the libraries used, the intermediate data produced, as well as the code generating tables and plots are presented in the statistical analysis section (SA) in the Supporting Information. The full R script and data set has been released in a public repository (https://doi.org/10.5281/zenodo.4297843).

■ ASSOCIATED CONTENT

Supporting Information

The Supporting Information is available free of charge at https://pubs.acs.org/doi/10.1021/acscatal.0c05294.

Protein production, electrochemical characterization, modeling, and statistical analysis (PDF)

■ AUTHOR INFORMATION

Corresponding Author

Roland Ludwig − *Biocatalysis and Biosensing Research Group, Department of Food Science and Technology, BOKU−University of Natural Resources and Life Sciences, 1190 Vienna, Austria;* orcid.org/0000-0002-5058-5874; Phone: +431 47654 75216; Email: roland.ludwig@boku.ac.at

Authors

Alfons K. G. Felice − *Biocatalysis and Biosensing Research Group, Department of Food Science and Technology, BOKU−University of Natural Resources and Life Sciences, 1190 Vienna, Austria*

Christian Schuster − *Biocatalysis and Biosensing Research Group, Department of Food Science and Technology, BOKU−University of Natural Resources and Life Sciences, 1190 Vienna, Austria*

Alan Kadek − *BIOCEV−Institute of Microbiology, The Czech Academy of Sciences, 252 50 Vestec, Czech Republic; Department of Biochemistry, Faculty of Science, Charles University in Prague, 128 43 Prague, Czech Republic*

Frantisek Filandr − *BIOCEV−Institute of Microbiology, The Czech Academy of Sciences, 252 50 Vestec, Czech Republic; Department of Biochemistry, Faculty of Science, Charles University in Prague, 128 43 Prague, Czech Republic*

Christophe V. F. P. Laurent − *Biocatalysis and Biosensing Research Group, Department of Food Science and Technology and Department of Material Sciences and Process Engineering, BOKU−University of Natural Resources and*

Life Sciences, 1190 Vienna, Austria; orcid.org/0000-0002-9112-6981

Stefan Scheiblbrandner − *Biocatalysis and Biosensing Research Group, Department of Food Science and Technology, BOKU−University of Natural Resources and Life Sciences, 1190 Vienna, Austria*

Lorenz Schwaiger − *Biocatalysis and Biosensing Research Group, Department of Food Science and Technology, BOKU−University of Natural Resources and Life Sciences, 1190 Vienna, Austria*

Franziska Schachinger − *Biocatalysis and Biosensing Research Group, Department of Food Science and Technology, BOKU−University of Natural Resources and Life Sciences, 1190 Vienna, Austria*

Daniel Kracher − *Biocatalysis and Biosensing Research Group, Department of Food Science and Technology, BOKU−University of Natural Resources and Life Sciences, 1190 Vienna, Austria*

Christoph Sygmund − *Biocatalysis and Biosensing Research Group, Department of Food Science and Technology, BOKU−University of Natural Resources and Life Sciences, 1190 Vienna, Austria*

Petr Man − *BIOCEV−Institute of Microbiology, The Czech Academy of Sciences, 252 50 Vestec, Czech Republic; Department of Biochemistry, Faculty of Science, Charles University in Prague, 128 43 Prague, Czech Republic*

Petr Halada − *BIOCEV−Institute of Microbiology, The Czech Academy of Sciences, 252 50 Vestec, Czech Republic*

Chris Oostenbrink − *Department of Material Sciences and Process Engineering, BOKU−University of Natural Resources and Life Sciences, 1190 Vienna, Austria;* orcid.org/0000-0002-4232-2556

Complete contact information is available at: https://pubs.acs.org/10.1021/acscatal.0c05294

Author Contributions

A.K.G.F. wrote the first draft of the manuscript and performed together with Christian Schuster and Christoph Sygmund the production and purification of chimeric CDHs and steady-state kinetic measurements. C.V.F.P.L. and C.O. performed and interpreted docking and modeling studies. A.K., F.F., P.M., and P.H. performed and analyzed H/D exchange experiments, A.K.G.F. and D.K. performed and analyzed fast-kinetic experiments, S.S., A.K.G.F, L.S., and F.S. performed and analyzed electrochemical experiments. R.L. initiated the study, designed experiments, evaluated and interpreted data, and wrote the final draft of the manuscript together with C.O, P.M., and P.H.

Funding

This work was funded by the Austrian Science Fund (project I2385-N28) and the Czech Science Foundation (projects 16-34818L) and the Europeans Union's Horizon 2020 research and innovation programme (ERC Consolidator Grant OXIDISE) under grant agreement no. 726396. A.K.G.F. was supported by a scholarship of the Austrian Academy of Sciences (DOC scholarship), S.S. by the MBW FM (Austrian Federal Ministry of Science, Research and Economy) International Graduate School BioNano Technology (IGS BioNano Tech) and C.V.F.P.L., L.S., F.S., and D.K. by the doctoral programme BioToP (W1224) funded by the Austrian Science Fund. A.K.G.F. was supported by a Doc fellowship of the Austrian Academy of Science. Access to the MS facility was enabled by MEYS CR (CZ.1.05/1.1.00/02.0109, LQ1604 and LM2015043 CIISB) funding.

Notes

The authors declare no competing financial interest.

■ ACKNOWLEDGMENTS

Daniela Gamperl is acknowledged for her fantastic work to produce chimeric CDH_{ABA}.

■ ABBREVIATIONS

AFM, atomic force microscopy; CDH, cellobiose dehydrogenase; CYT, cytochrome domain; DCIP, 2,6-dichloroindophenol; DH, dehydrogenase domain; FAD, flavin adenine dinucleotide; HDX, hydrogen/deuterium exchange; IDET, interdomain electron transfer; IPET, interprotein electron transfer; LPMO, lytic polysaccharide monooxygenase; MS, mass spectrometry; SAM, self-assembled monolayer; SANS, small-angle neutron scattering; SAXS, small-angle X-ray scattering; SHE, standard hydrogen electrode; TN, turnover number

■ REFERENCES

(1) Langston, J. A.; Shaghasi, T.; Abbate, E.; Xu, F.; Vlasenko, E.; Sweeney, M. D. Oxidoreductive Cellulose Depolymerization by the Enzymes Cellobiose Dehydrogenase and Glycoside Hydrolase 61. *Appl. Environ. Microbiol.* **2011**, *77*, 7007−7015.

(2) Phillips, C. M.; Beeson, W. T.; Cate, J. H.; Marletta, M. A. Cellobiose Dehydrogenase and a Copper-Dependent Polysaccharide Monooxygenase Potentiate Cellulose Degradation by *Neurospora crassa*. *ACS Chem. Biol.* **2011**, *6*, 1399−1406.

(3) Phillips, C. M.; Iavarone, A. T.; Marletta, M. A. Quantitative Proteomic Approach for Cellulose Degradation by *Neurospora crassa*. *J. Proteome Res.* **2011**, *10*, 4177−4185.

(4) Harris, P. V.; Welner, D.; McFarland, K. C.; Re, E.; Navarro Poulsen, J.-C.; Brown, K.; Salbo, R.; Ding, H.; Vlasenko, E.; Merino, S.; Xu, F.; Cherry, J.; Larsen, S.; Lo Leggio, L. Stimulation of Lignocellulosic Biomass Hydrolysis by Proteins of Glycoside Hydrolase Family 61: Structure and Function of a Large, Enigmatic Family. *Biochemistry* **2010**, *49*, 3305−3316.

(5) Quinlan, R. J.; Sweeney, M. D.; Lo Leggio, L.; Otten, H.; Poulsen, J.-C. N.; Johansen, K. S.; Krogh, K. B. R. M.; Jorgensen, C. I.; Tovborg, M.; Anthonsen, A.; Tryfona, T.; Walter, C. P.; Dupree, P.; Xu, F.; Davies, G. J.; Walton, P. H. Insights into the Oxidative Degradation of Cellulose by a Copper Metalloenzyme That Exploits Biomass Components. *Proc. Natl. Acad. Sci. U.S.A.* **2011**, *108*, 15079−15084.

(6) Kracher, D.; Scheiblbrandner, S.; Felice, A. K. G.; Breslmayr, E.; Preims, M.; Ludwicka, K.; Haltrich, D.; Eijsink, V. G. H.; Ludwig, R. Extracellular Electron Transfer Systems Fuel Cellulose Oxidative Degradation. *Science* **2016**, *352*, 1098−1101.

(7) Sygmund, C.; Kracher, D.; Scheiblbrandner, S.; Zahma, K.; Felice, A. K. G.; Harreither, W.; Kittl, R.; Ludwig, R. Characterization of the Two *Neurospora crassa* Cellobiose Dehydrogenases and Their Connection to Oxidative Cellulose Degradation. *Appl. Environ. Microbiol.* **2012**, *78*, 6161−6171.

(8) Igarashi, K.; Yoshida, M.; Matsumura, H.; Nakamura, N.; Ohno, H.; Samejima, M.; Nishino, T. Electron Transfer Chain Reaction of the Extracellular Flavocytochrome Cellobiose Dehydrogenase from the Basidiomycete *Phanerochaete chrysosporium*. *FEBS J.* **2005**, *272*, 2869−2877.

(9) Tan, T.-C.; Kracher, D.; Gandini, R.; Sygmund, C.; Kittl, R.; Haltrich, D.; Hällberg, B. M.; Ludwig, R.; Divne, C. Structural Basis for Cellobiose Dehydrogenase Action during Oxidative Cellulose Degradation. *Nat. Commun.* **2015**, *6*, 7542.

(10) Igarashi, K.; Momohara, I.; Nishino, T.; Samejima, M. Kinetics of Inter-Domain Electron Transfer in Flavocytochrome Cellobiose

Dehydrogenase from the White-Rot Fungus *Phanerochaete chrysosporium*. *Biochem. J.* **2002**, *365*, 521.
(11) Kracher, D.; Zahma, K.; Schulz, C.; Sygmund, C.; Gorton, L.; Ludwig, R. Inter-Domain Electron Transfer in Cellobiose Dehydrogenase: Modulation by pH and Divalent Cations. *FEBS J.* **2015**, *282*, 3136−3148.
(12) Bodenheimer, A. M.; O'Dell, W. B.; Oliver, R. C.; Qian, S.; Stanley, C. B.; Meilleur, F. Structural Investigation of Cellobiose Dehydrogenase IIA: Insights from Small Angle Scattering into Intra- and Intermolecular Electron Transfer Mechanisms. *Biochim. Biophys. Acta, Gen. Subj.* **2018**, *1862*, 1031−1039.
(13) Bodenheimer, A. M.; O'Dell, W. B.; Stanley, C. B.; Meilleur, F. Structural Studies of *Neurospora crassa* LPMO9D and Redox Partner CDHIIA Using Neutron Crystallography and Small-Angle Scattering. *Carbohydr. Res.* **2017**, *448*, 200−204.
(14) Harada, H.; Onoda, A.; Uchihashi, T.; Watanabe, H.; Sunagawa, N.; Samejima, M.; Igarashi, K.; Hayashi, T. Interdomain Flip-Flop Motion Visualized in Flavocytochrome Cellobiose Dehydrogenase Using High-Speed Atomic Force Microscopy during Catalysis. *Chem. Sci.* **2017**, *8*, 6561−6565.
(15) Courtade, G.; Wimmer, R.; Røhr, Å. K.; Preims, M.; Felice, A. K. G.; Dimarogona, M.; Vaaje-Kolstad, G.; Sørlie, M.; Sandgren, M.; Ludwig, R.; Eijsink, V. G. H.; Aachmann, F. L. Interactions of a Fungal Lytic Polysaccharide Monooxygenase with β-Glucan Substrates and Cellobiose Dehydrogenase. *Proc. Natl. Acad. Sci. U.S.A.* **2016**, *113*, 5922−5927.
(16) Laurent, C. V. F. P.; Breslmayr, E.; Tunega, D.; Ludwig, R.; Oostenbrink, C. Interaction between Cellobiose Dehydrogenase and Lytic Polysaccharide Monooxygenase. *Biochemistry* **2019**, *58*, 1226−1235.
(17) Ortiz, R.; Matsumura, H.; Tasca, F.; Zahma, K.; Samejima, M.; Igarashi, K.; Ludwig, R.; Gorton, L. Effect of Deglycosylation of Cellobiose Dehydrogenases on the Enhancement of Direct Electron Transfer with Electrodes. *Anal. Chem.* **2012**, *84*, 10315−10323.
(18) Hallberg, B. M.; Henriksson, G.; Pettersson, G.; Divne, C. Crystal Structure of the Flavoprotein Domain of the Extracellular Flavocytochrome Cellobiose Dehydrogenase. *J. Mol. Biol.* **2002**, *315*, 421−434.
(19) Zamocky, M.; Ludwig, R.; Peterbauer, C.; Hallberg, B.; Divne, C.; Nicholls, P.; Haltrich, D. Cellobiose Dehydrogenase-a Flavocytochrome from Wood-Degrading, Phytopathogenic and Saprotropic Fungi. *Curr. Protein Pept. Sci.* **2006**, *7*, 255−280.
(20) Mason, M. G.; Wilson, M. T.; Ball, A.; Nicholls, P. Oxygen Reduction by Cellobiose Oxidoreductase: The Role of the Haem Group. *FEBS Lett.* **2002**, *518*, 29−32.
(21) Mason, M. G.; Nicholls, P.; Divne, C.; Hallberg, B. M.; Henriksson, G.; Wilson, M. T. The Heme Domain of Cellobiose Oxidoreductase: A One-Electron Reducing System. *Biochim. Biophys. Acta, Rev. Bioenerg.* **2003**, *1604*, 47−54.
(22) Samejima, M.; Phillips, R. S.; Eriksson, K.-E. L. Cellobiose Oxidase from *Phanerochaete chrysosporium* Stopped-Flow Spectrophotometric Analysis of pH-Dependent Reduction. *FEBS Lett.* **1992**, *306*, 165−168.
(23) Moser, C. C.; Keske, J. M.; Warncke, K.; Farid, R. S.; Dutton, P. L. Nature of Biological Electron Transfer. *Nature* **1992**, *355*, 796−802.
(24) Page, C. C.; Moser, C. C.; Chen, X.; Dutton, P. L. Natural Engineering Principles of Electron Tunnelling in Biological Oxidation−Reduction. *Nature* **1999**, *402*, 47−52.
(25) Dominguez, C.; Boelens, R.; Bonvin, A. M. J. J. HADDOCK: A Protein−Protein Docking Approach Based on Biochemical or Biophysical Information. *J. Am. Chem. Soc.* **2003**, *125*, 1731−1737.
(26) de Vries, S. J.; van Dijk, A. D. J.; Krzeminski, M.; van Dijk, M.; Thureau, A.; Hsu, V.; Wassenaar, T.; Bonvin, A. M. J. J. HADDOCK versus HADDOCK: New Features and Performance of HADDOCK2.0 on the CAPRI Targets. *Proteins: Struct., Funct., Bioinf.* **2007**, *69*, 726−733.
(27) Eichenberger, A. P.; Allison, J. R.; Dolenc, J.; Geerke, D. P.; Horta, B. A. C.; Meier, K.; Oostenbrink, C.; Schmid, N.; Steiner, D.; Wang, D.; van Gunsteren, W. F. GROMOS++ Software for the Analysis of Biomolecular Simulation Trajectories. *J. Chem. Theory Comput.* **2011**, *7*, 3379−3390.
(28) de Ruiter, A.; Oostenbrink, C. Protein−Ligand Binding from Distancefield Distances and Hamiltonian Replica Exchange Simulations. *J. Chem. Theory Comput.* **2013**, *9*, 883−892.
(29) Xue, L. C.; Rodrigues, J. P.; Kastritis, P. L.; Bonvin, A. M.; Vangone, A. PRODIGY: A Web Server for Predicting the Binding Affinity of Protein-Protein Complexes. *Bioinformatics* **2016**, *32*, 3676−3678.
(30) Kastritis, P. L.; Rodrigues, J. P. G. L. M.; Folkers, G. E.; Boelens, R.; Bonvin, A. M. J. J. Proteins Feel More Than They See: Fine-Tuning of Binding Affinity by Properties of the Non-Interacting Surface. *J. Mol. Biol.* **2014**, *426*, 2632−2652.
(31) Vangone, A.; Bonvin, A. M. Contacts-Based Prediction of Binding Affinity in Protein-Protein Complexes. *eLife* **2015**, *4*, No. e07454.
(32) Janin, J.; Bahadur, R. P.; Chakrabarti, P. Protein−Protein Interaction and Quaternary Structure. *Q. Rev. Biophys.* **2008**, *41*, 133−180.
(33) Li, X.; Beeson, W. T.; Phillips, C. M.; Marletta, M. A.; Cate, J. H. D. Structural Basis for Substrate Targeting and Catalysis by Fungal Polysaccharide Monooxygenases. *Structure* **2012**, *20*, 1051−1061.
(34) Kittl, R.; Kracher, D.; Burgstaller, D.; Haltrich, D.; Ludwig, R. Production of Four *Neurospora crassa* Lytic Polysaccharide Monooxygenases in Pichia Pastoris Monitored by a Fluorimetric Assay. *Biotechnol. Biofuels* **2012**, *5*, 79.
(35) Kadek, A.; Kavan, D.; Felice, A. K. G.; Ludwig, R.; Halada, P.; Man, P. Structural Insight into the Calcium Ion Modulated Interdomain Electron Transfer in Cellobiose Dehydrogenase. *FEBS Lett.* **2015**, *589*, 1194−1199.
(36) Konermann, L.; Vahidi, S.; Sowole, M. A. Mass Spectrometry Methods for Studying Structure and Dynamics of Biological Macromolecules. *Anal. Chem.* **2014**, *86*, 213−232.
(37) Sowole, M. A.; Konermann, L. Effects of Protein−Ligand Interactions on Hydrogen/Deuterium Exchange Kinetics: Canonical and Noncanonical Scenarios. *Anal. Chem.* **2014**, *86*, 6715−6722.
(38) Lindgren, A.; Larsson, T.; Ruzgas, T.; Gorton, L. Direct Electron Transfer between the Heme of Cellobiose Dehydrogenase and Thiol Modified Gold Electrodes. *J. Electroanal. Chem.* **2000**, *494*, 105−113.
(39) Nicholson, R. S. Theory and Application of Cyclic Voltammetry for Measurement of Electrode Reaction Kinetics. *Anal. Chem.* **1965**, *37*, 1351−1355.
(40) Bowden, E. F.; Hawkridge, F. M.; Blount, H. N. Interfacial Electrochemistry of Cytochrome c at Tin Oxide, Indium Oxide, Gold, and Platinum Electrodes. *J. Electroanal. Chem. Interfacial Electrochem.* **1984**, *161*, 355−376.
(41) Raices, M.; Paifer, E.; Cremata, J.; Montesino, R.; Ståhlberg, J.; Divne, C.; Szabó, I. J.; Henriksson, G.; Johansson, G.; Pettersson, G. Cloning and Characterization of a CDNA Encoding a Cellobiose Dehydrogenase from the White Rot Fungus *Phanerochaete chrysosporium*. *FEBS Lett.* **1995**, *369*, 233−238.
(42) Hallberg, B. M.; Bergfors, T.; Bäckbro, K.; Pettersson, G.; Henriksson, G.; Divne, C. A New Scaffold for Binding Haem in the Cytochrome Domain of the Extracellular Flavocytochrome Cellobiose Dehydrogenase. *Structure* **2000**, *8*, 79−88.
(43) Diêp Lê, K. H.; Lederer, F.; Golinelli-Pimpaneau, B. Structural Evidence for the Functional Importance of the Heme Domain Mobility in Flavocytochrome b2. *J. Mol. Biol.* **2010**, *400*, 518−530.
(44) Vaaje-Kolstad, G.; Westereng, B.; Horn, S. J.; Liu, Z.; Zhai, H.; Sørlie, M.; Eijsink, V. G. H. An Oxidative Enzyme Boosting the Enzymatic Conversion of Recalcitrant Polysaccharides. *Science* **2010**, *330*, 219−222.
(45) Kadek, A.; Kavan, D.; Marcoux, J.; Stojko, J.; Felice, A. K. G.; Cianférani, S.; Ludwig, R.; Halada, P.; Man, P. Interdomain Electron Transfer in Cellobiose Dehydrogenase Is Governed by Surface Electrostatics. *Biochim. Biophys. Acta, Gen. Subj.* **2017**, *1861*, 157−167.

https://dx.doi.org/10.1021/acscatal.0c05294
ACS Catal. 2021, 11, 517−532

(46) Harreither, W.; Sygmund, C.; Augustin, M.; Narciso, M.; Rabinovich, M. L.; Gorton, L.; Haltrich, D.; Ludwig, R. Catalytic Properties and Classification of Cellobiose Dehydrogenases from Ascomycetes. *Appl. Environ. Microbiol.* **2011**, *77*, 1804−1815.
(47) Jones, S. M.; Transue, W. J.; Meier, K. K.; Kelemen, B.; Solomon, E. I. Kinetic Analysis of Amino Acid Radicals Formed in H_2O_2-Driven CuI LPMO Reoxidation Implicates Dominant Homolytic Reactivity. *Proc. Natl. Acad. Sci. U.S.A.* **2020**, *117*, 11916−11922.
(48) Paradisi, A.; Johnston, E. M.; Tovborg, M.; Nicoll, C. R.; Ciano, L.; Dowle, A.; McMaster, J.; Hancock, Y.; Davies, G. J.; Walton, P. H. Formation of a Copper(II)−Tyrosyl Complex at the Active Site of Lytic Polysaccharide Monooxygenases Following Oxidation by H_2O_2. *J. Am. Chem. Soc.* **2019**, *141*, 18585−18599.
(49) Chylenski, P.; Bissaro, B.; Sørlie, M.; Røhr, Å. K.; Várnai, A.; Horn, S. J.; Eijsink, V. G. H. Lytic Polysaccharide Monooxygenases in Enzymatic Processing of Lignocellulosic Biomass. *ACS Catal.* **2019**, *9*, 4970−4991.
(50) Petrović, D. M.; Várnai, A.; Dimarogona, M.; Mathiesen, G.; Sandgren, M.; Westereng, B.; Eijsink, V. G. H. Comparison of Three Seemingly Similar Lytic Polysaccharide Monooxygenases from *Neurospora crassa* Suggests Different Roles in Plant Biomass Degradation. *J. Biol. Chem.* **2019**, *294*, 15068−15081.
(51) Loose, J. S. M.; Forsberg, Z.; Kracher, D.; Scheiblbrandner, S.; Ludwig, R.; Eijsink, V. G. H.; Vaaje-Kolstad, G. Activation of Bacterial Lytic Polysaccharide Monooxygenases with Cellobiose Dehydrogenase. *Protein Sci.* **2016**, *25*, 2175−2186.
(52) Tamura, K.; Stecher, G.; Peterson, D.; Filipski, A.; Kumar, S. MEGA6: Molecular Evolutionary Genetics Analysis Version 6.0. *Mol. Biol. Evol.* **2013**, *30*, 2725−2729.
(53) Harreither, W.; Felice, A. K. G.; Paukner, R.; Gorton, L.; Ludwig, R.; Sygmund, C. Recombinantly Produced Cellobiose Dehydrogenase from *Corynascus thermophilus* for Glucose Biosensors and Biofuel Cells. *Biotechnol. J.* **2012**, *7*, 1359−1366.
(54) Weis, R.; Luiten, R.; Skranc, W.; Schwab, H.; Wubbolts, M.; Glieder, A. Reliable High-Throughput Screening with Pichia Pastoris by Limiting Yeast Cell Death Phenomena. *FEMS Yeast Res.* **2004**, *5*, 179−189.
(55) McIlvaine, T. C. A Buffer Solution for Colorimetric Comparison. *J. Biol. Chem.* **1921**, *49*, 183−186.
(56) Gasteiger, E.; Hoogland, C.; Gattiker, A.; Duvaud, S.; Wilkins, M. R.; Appel, R. D.; Bairoch, A. Protein Identification and Analysis Tools on the ExPASy Server. In *The Proteomics Protocols Handbook*; Walker, J. M., Ed.; Humana Press: Totowa, NJ, 2005; pp 571−607.
(57) Nicholson, R. S.; Shain, I. Theory of Stationary Electrode Polarography. Single Scan and Cyclic Methods Applied to Reversible, Irreversible, and Kinetic Systems. *Anal. Chem.* **1964**, *36*, 706−723.
(58) Matsuda, H. Zur Theorie der Wechselspannungs-Polarographie. *Z. für Elektrochem. Berichte Bunsenges. für Phys. Chem.* **1958**, *62*, 977−989.
(59) Ševčík, A. Oscillographic Polarography with Periodical Triangular Voltage. *Collect. Czech. Chem. Commun.* **1948**, *13*, 349−377.
(60) Randles, J. E. B. A Cathode Ray Polarograph Part II.—The Current-Voltage Curves. *Trans. Faraday Soc.* **1948**, *44*, 327−338.
(61) Arnold, K.; Bordoli, L.; Kopp, J.; Schwede, T. The SWISS-MODEL Workspace: A Web-Based Environment for Protein Structure Homology Modelling. *Bioinformatics* **2006**, *22*, 195−201.
(62) Benkert, P.; Biasini, M.; Schwede, T. Toward the Estimation of the Absolute Quality of Individual Protein Structure Models. *Bioinformatics* **2011**, *27*, 343−350.
(63) Biasini, M.; Bienert, S.; Waterhouse, A.; Arnold, K.; Studer, G.; Schmidt, T.; Kiefer, F.; Cassarino, T. G.; Bertoni, M.; Bordoli, L.; Schwede, T. SWISS-MODEL: Modelling Protein Tertiary and Quaternary Structure Using Evolutionary Information. *Nucleic Acids Res.* **2014**, *42*, W252−W258.
(64) Schmid, N.; Christ, C. D.; Christen, M.; Eichenberger, A. P.; van Gunsteren, W. F. Architecture, Implementation and Parallelisation of the GROMOS Software for Biomolecular Simulation. *Comput. Phys. Commun.* **2012**, *183*, 890−903.
(65) Schmid, N.; Eichenberger, A. P.; Choutko, A.; Riniker, S.; Winger, M.; Mark, A. E.; van Gunsteren, W. F. Definition and Testing of the GROMOS Force-Field Versions 54A7 and 54B7. *Eur. Biophys. J.* **2011**, *40*, 843−856.
(66) Poger, D.; Van Gunsteren, W. F.; Mark, A. E. A New Force Field for Simulating Phosphatidylcholine Bilayers. *J. Comput. Chem.* **2010**, *31*, 1117−1125.
(67) Olsson, M. H. M.; Søndergaard, C. R.; Rostkowski, M.; Jensen, J. H. PROPKA3: Consistent Treatment of Internal and Surface Residues in Empirical pKa Predictions. *J. Chem. Theory Comput.* **2011**, *7*, 525−537.
(68) Søndergaard, C. R.; Olsson, M. H. M.; Rostkowski, M.; Jensen, J. H. Improved Treatment of Ligands and Coupling Effects in Empirical Calculation and Rationalization of pKa Values. *J. Chem. Theory Comput.* **2011**, *7*, 2284−2295.
(69) Dolinsky, T. J.; Nielsen, J. E.; McCammon, J. A.; Baker, N. A. PDB2PQR: An Automated Pipeline for the Setup of Poisson−Boltzmann Electrostatics Calculations. *Nucleic Acids Res.* **2004**, *32*, W665−W667.
(70) Baker, N. A.; Sept, D.; Joseph, S.; Holst, M. J.; McCammon, J. A. Electrostatics of Nanosystems: Application to Microtubules and the Ribosome. *Proc. Natl. Acad. Sci. U.S.A.* **2001**, *98*, 10037−10041.
(71) Bank, R. E.; Holst, M. A New Paradigm for Parallel Adaptive Meshing Algorithms. *SIAM Rev.* **2003**, *45*, 291−323.
(72) Holst, M. Adaptive Numerical Treatment of Elliptic Systems on Manifolds. *Adv. Comput. Math.* **2001**, *15*, 139−191.
(73) Holst, M.; Saied, F. Multigrid Solution of the Poisson—Boltzmann Equation. *J. Comput. Chem.* **1993**, *14*, 105−113.
(74) Holst, M. J.; Saied, F. Numerical Solution of the Nonlinear Poisson−Boltzmann Equation: Developing More Robust and Efficient Methods. *J. Comput. Chem.* **1995**, *16*, 337−364.
(75) Kastritis, P. L.; Rodrigues, J. P. G. L. M.; Folkers, G. E.; Boelens, R.; Bonvin, A. M. J. J. Proteins Feel More Than They See: Fine-Tuning of Binding Affinity by Properties of the Non-Interacting Surface. *J. Mol. Biol.* **2014**, *426*, 2632−2652.
(76) Vangone, A.; Bonvin, A. M. Contacts-Based Prediction of Binding Affinity in Protein−Protein Complexes. *eLife* **2015**, *4*, No. e07454.
(77) Xue, L. C.; Rodrigues, J. P.; Kastritis, P. L.; Bonvin, A. M.; Vangone, A. PRODIGY: A Web Server for Predicting the Binding Affinity of Protein−Protein Complexes. *Bioinformatics* **2016**, *32*, 3676−3678.
(78) Lê, S.; Josse, J.; Husson, F. FactoMineR: An R Package for Multivariate Analysis. *J. Stat. Software* **2008**, *25*, 1.
(79) Revelle, W. R. *Psych: Procedures for Personality and Psychological Research*, 2017.

https://dx.doi.org/10.1021/acscatal.0c05294
ACS Catal. 2021, 11, 517−532